Aalto-yliopisto
Insinööritieteiden
korkeakoulu

Olli Sarainmaa

Large Efficient Maritime Propeller without Hull Pressure Excitations

Diplomityö, joka on jätetty opinnäytteenä tarkastettavaksi diplomi-insinöörin tutkintoa varten.

Espoossa 13.11.2018
Valvojat: Professori Jani Romanoff
Ohjaajat: Hans Liwång, Raimo Hämäläinen

Aalto-yliopisto
Insinööritieteiden
korkeakoulu

Aalto University, P.O. BOX 11000, 00076 AALTO
www.aalto.fi

Abstract of master's thesis

Author Olli Sarainmaa

Title of thesis Large Efficient Maritime Propeller without Hull Pressure Excitations

Degree programme Nordic Master in Maritime Engineering

Major/minor Small Craft **Code** ENG214

Thesis supervisor Jani Romanoff

Thesis advisor(s) Hans Liwång, Raimo Hämäläinen

Date 13.11.2018 **Number of pages** 69 **Language** English

Abstract

This thesis studies competence of simplified simulation methods for boosting simulation. The most efficient propulsion unit has higher amount of power compared to less efficient propulsion units in boosting. Boosting is relevant subject to study due to new concept. New concept allows a larger diameter for the propeller which increases the efficiency of the propeller. New concept relies on the idea to have the propeller behind the hull.

The thesis is restricted to study displacement hulls from a point of view of propulsion efficiency. Large cruise ship model is utilized in this thesis to identify boosting related effects efficiently. Model tests reports of this concept are used as a baseline and a comparison material for two methods that are tested in this thesis. These methods are Matlab simulation code and OpenFOAM as the CFD software.

New propulsion arrangement concept is more efficient than current solutions for this hull type according to model tests. Trend of the CFD and Matlab simulation results matches well with model test results for boosting. Matlab simulation is evidently more time efficient solution than CFD simulation for boosting. Simplified CFD simulation is sufficiently accurate to study boosting concept with this research setup. Matlab and CFD simulations can be combined to obtain the most efficient solution to analyze the most effective load division for boosting.

Different types of hulls should be simulated and results should be verificated with model or full scale tests. In addition, ships with old two shaft arrangements could be converted to have two smaller pods and center line propeller in order to have better comparison with current methods. Scaling factors increases the uncertainty for new concepts; therefore full scale measurements are required.

Keywords CFD, propulsion, concept, boosting

Preface

This thesis is part of the Nordic Master in Maritime Engineering degree at Aalto University and KTH, Royal Institute of Technology. It is done for Meyer Turku shipyard. Basis for this research originally stemmed from my passion for hydrodynamics and Meyer Turku gave me an opportunity to do a research about an important subject. I have always enjoyed researching new concepts, less writing about them; therefore this thesis was an enormous mountain to be climbed on.

Acknowledgements

I want to give special thanks for Meyer Turku for giving opportunity to use their CFD calculation units and special thanks for Pekka Kanninen who helped with OpenFOAM simulations whenever I needed help. In addition, I want to thank Raimo Hämäläinen, head of hydrodynamics at Meyer Turku to give an opportunity to study a unique concept. I want to also thank the supervisors in both universities Hans Liwång at KTH and Jani Romanoff at Aalto University who helped me during the thesis, especially in fine tuning the thesis.

Table of contents

List of Figures

List of Tables

Nomenclature

A_0	[-]	Cross-section area of the propeller
C_A	[-]	Correlation allowance
C_F	[-]	Friction coefficient
C_R	[-]	Residual coefficient
C_T	[-]	Total resistance coefficient
d	[m]	Diameter of the propeller
F_D	[N]	Viscous scale effect on resistance
F_n	[-]	Froude's number
J	[-]	Advance coefficient
K_T	[-]	Thrust coefficient
K_Q	[-]	Torque coefficient
k	[-]	Form factor
L	[m]	Length of the ship
n	[1/s]	Number of revolutions
P_B	[W]	Brake power
P_D	[W]	Delivered power
P_E	[W]	Effective power
P_T	[W]	Thrust power
R_F	[N]	Friction resistance
R_P	[N]	Pressure resistance
R_T	[N]	Total resistance
S	[m^2]	Wetter surface area of the ship
T	[N]	Thrust
t	[-]	Thrust deduction factor
V_a	[m/s]	Advanced velocity of the propeller
V	[m/s]	Velocity of the ship
w	[-]	Wake fraction coefficient
Q	[Nm]	Torque
ρ	[kg/m^3]	Density of water
η_B	[-]	Propulsive efficiency
η_H	[-]	Hull efficiency
η_O	[-]	Open water efficiency
η_R	[-]	Rotative efficiency
η_S	[-]	Shaft efficiency
η_T	[-]	Total efficiency
λ	[-]	Scale ratio

Abbreviations

CFD	Computational Fluid Dynamics
GT	Gross Tonnage
FVM	Finite Volume Method
HFO	Heavy Fuel Oil
IMO	International Maritime Organization
LTS	Local Time-Steping
MARIN	Maritime Research Institute Netherlands
MCR	Maximum Continuous Rating
RANS	Reynolds-Averaged Navier-Stokes
RPM	Revolutions Per Minute
OpenFOAM	Open Source Field Operation And Manipulation
PISO	Pressure Implicit with Splitting of Operator
SFC	Specific Fuel Consumption
SIMPLE	Semi-Implicit Method for Pressure-Linked Equations
SST	Shear Stress Transport
TVD	Total Variation Diminishing
VOF	Volume of Fluid

1 Introduction and Background

New concept of large centerline propeller that is behind the hull is the foundation for this thesis. This concept provides more efficient propulsion without hull pressure excitations. This effect is emphasized with a concept of boosting. These concepts introduce better propulsion efficiency. This work focuses on studying boosting aspect of this new concept from the perspective of energy efficient hydrodynamics for displacement hulls. Hypothesis is that trends of different boosting situations can be modelled with simple methods. Object is to define two simple methods to model boosting with means of CFD and Matlab simulation code for concept phase of the design. Both of the methods are calibrated with results from model test. In addition, CFD simulation is calibrated with results from Matlab simulation that does not require model test information necessary. These methods are compared to model test results that are done prior to this thesis, since model tests are considered as the most reliable way to predict performance. Large cruise ship model is used to make effortless to identify boosting related aspects.

Boosting requires at least three propulsion units and therefore new propulsion concept is introduced. Small crafts and their propulsion design is the source of inspiration for the new concept.

Thesis is divided to five main sections. First introduces the problem and gives motivation why it is an important subject. Second section introduces the main methods and their theory related to this thesis. Third section introduces the results that are found during this thesis. Fourth section is a discussion section that concludes the thesis. Last section is what to do in the future.

1.1 Motivation

There is a constant pressure to develop ships more efficient. Hull form and its appendages are the best energy saving possibilities. Design of these affects the whole lifetime of the vessel and makes competition effortless in tough markets as indicated in the energy saving possibilities study for cruise ships study [1]. It is noted in the conclusion of the report [2] that state-of-the-art techniques allow the optimization of the propulsion arrangement and the most effective efficiency measures to save propulsion power in the early phase of the design. Especially, with larger ships small improvements in the efficiency can lead to high fuel savings per year. Significance of improvements is increasing since fuel price is constantly increasing (Figure 1). In addition, environmental regulations will be stricter in the future as shown in the IMO publication [3].

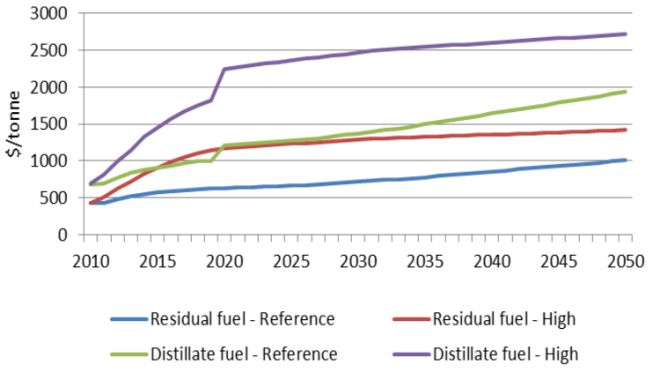

Figure 1 Fuel price scenarios [4]

In the ship design resources are always limited. Complex simulation requires more computational power. It is important to lock down decisions as early as possible as it is easier to modify features when design is in early phase (Figure 2). In addition, it is important to evaluate different design aspects to achieve the most effective design; therefore it is important to have cost and time effective solution. In the later stage results of simpler model can be verificate with more accurate model.

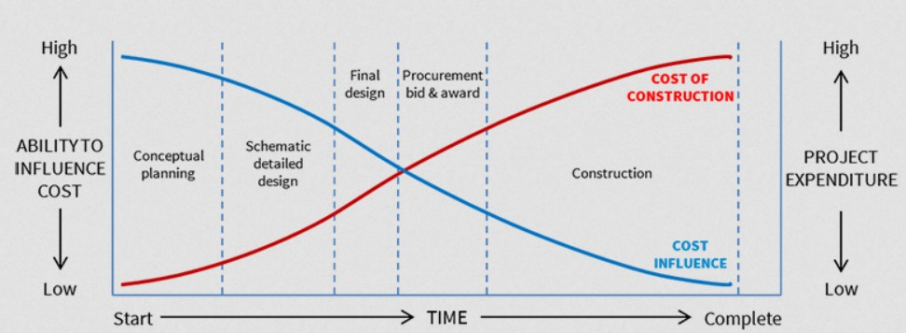

Figure 2 Cost influence curve [5]

1.1.1 Benchmarking Small Craft

There is no straight-forward definition for a small craft, however United States Coast Guard has rather simple definition for this: "Small craft is a vessel sixty-five feet or less in length" as shown in the Small Craft Facility Training Guide [6]. 65 feet is approximately 19.8 meters. Due to size restriction boosting is not relevant with displacement small crafts since it is not energy efficient to have three propulsion units in small slow speed vessel.

Propeller behind the hull is not uncommon with small crafts. Smaller crafts usually have higher Froude number, which means that they are usually semi-displacement or planning crafts (Figure 3). Some aspects of semi-displacement and planning crafts are introduced in order to clarify what a displacement craft is.

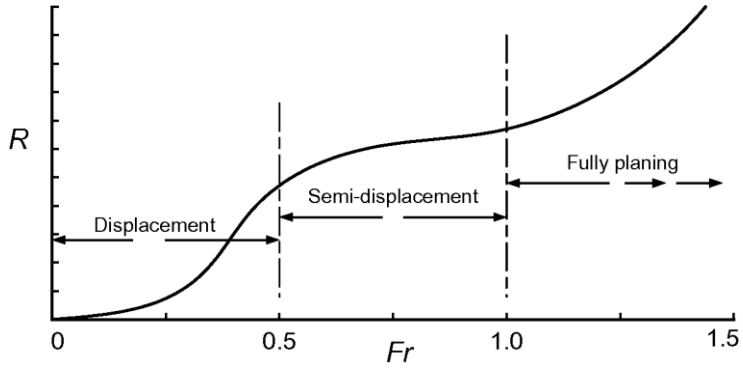

Figure 3 Resistance versus Speed/Length ratio [7]

The principle difference with displacement and planning and semi-displacement hulls is that displacement hull has only buoyancy force and gravity that are balanced. Semi-displacement and planning hulls have lift force as an additional force that modifies the hydrodynamic analysis significantly.

Displacement hulls are usually large, round and bulbous. They are relatively slow as speed is limited by its waterline length, since bow wave that vessel creates is forming a barrier for higher speed. Semi displacement hull is a cross between a planning and displacement

hull, they generate some lift but in the end vessel weight is supported by buoyancy. These kinds of hulls create a large hole in the water which generates large bow and stern waves. These hulls are similar to displacement hulls although will flatten towards the stern to form a planning effect. A planning hull is designed to generate lift. This kind of craft surfs on its own bow wave and decreases its draft with speed, when draft is decreased it decreases the wetted surface and therefore viscous resistance.

There are different propulsion concepts with yachts and small crafts, where propeller is behind the hull. One as an example is a surface drive. This type of propulsion is the most similar with concept introduced in this thesis. Propeller is behind the hull and is covered with a plate.

Figure 4 Surface drive [8]

1.2 Application to Larger Vessels

Larger vessels in this context are displacement vessels that are larger than small craft and have at least three propulsion units.

Hybrid propulsion concept that can be utilized for boosting can be used with various types of vessels. Motor yachts can utilize three pod units, two pod units and center line propeller, two shaft units and waterjet or three shaft units. There are few super yachts that already uses concept of twin screw with additional waterjet. One of these examples is Ecstasea (Figure 5), which is 86 meter motor yacht built in 2004 as shown in the [9].

Figure 5 Ecstasea yacht with twin screw and waterjet [9]

Finnish offshore patrol vessel Turva uses the similar type of propulsion system as in this thesis. It has two azimuth propulsion units and one centerline propeller as shown in the [10]. In this vessel centerline propeller is under the hull.

One notable concept to be combined with this concept is a retractable propulsion system (Figure 6). It is introduced in Baltic 130 Custom sailing yacht as shown in the [11]. One of the major benefits is that in different operational modes propeller can be taken inside of the hull when resistance is significantly lower as propeller is not dragging. This idea can be used with motor yachts as they can have waterjet and pods, then they could retractable either waterjet or pods to use the most optimum propulsion arrangement in various speed range.

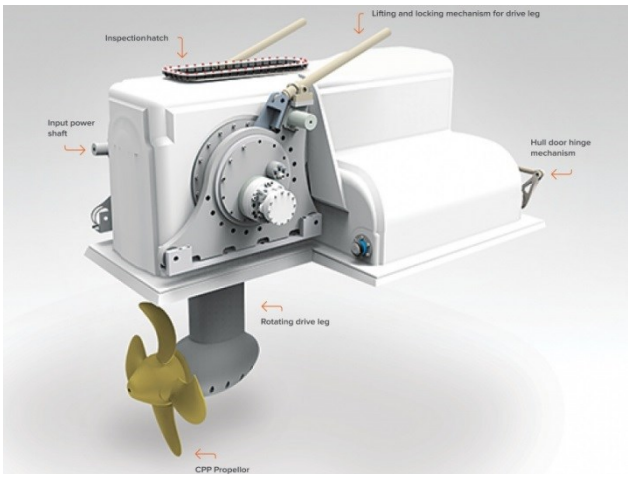

Figure 6 Retractable propulsion system from Baltic Yachts [11]

Features from the hybrid propulsion and small crafts are combined. It leads to a new concept, where centerline propeller is behind the hull as in small crafts (Figure 7). In addition, there are two side pod units. This hybrid propulsion delivers two major benefits for the vessel. It allows increasing the diameter of the propeller, which increases efficiency in theory. This allows boosting high efficiency propeller to increase efficiency further. In addition, it improves comfort in the ship, as propeller induced hull pressure excitations decreases significantly as propeller is not under the hull. This is proven with model tests that hull-pressure fluctuations are extremely low, closing to zero as described in the model test report [12].

Figure 7 The model with new propulsion concept

New concept introduces new issues. Some of these issues were assumed to be ventilation and safety, since propeller tip is closer to surface. Tip of the blade may suck air into propeller due to pressure difference, this might lead to cavitation issues, however it was proved not to be an issue with model tests as described in [12]. There is a higher risk for other vessels to hit the propeller as it is not covered with the hull, however the area of the propeller can be covered with a plate without water connection as discussed with Raimo Hämäläinen [13]. Larger diameter for same amount of thrust leads to lower RPM. It leads to higher shaft torque, which leads to larger shafts and gearboxes. However, this thesis focuses only on the hydrodynamic efficiency of the concept.

Different matters are affecting on an optimum propeller design such as RPM, number of blades, blade outline, camber, angle of attack, pitch diameter –ratio and diameter. Larger diameter allows more efficient propulsive as shown in the [14]. In theory, lower thrust loading coefficient means higher efficiency (Figure 8) as shown in the [15]

$$C_T = \frac{P_D}{\frac{1}{2}\rho A_0 V_A^3}. \quad (1)$$

Cross-section area of the propeller (A_0) has great influence on this coefficient as shown in the equation (1); therefore larger diameter leads to lower thrust loading factor and thus higher efficiency

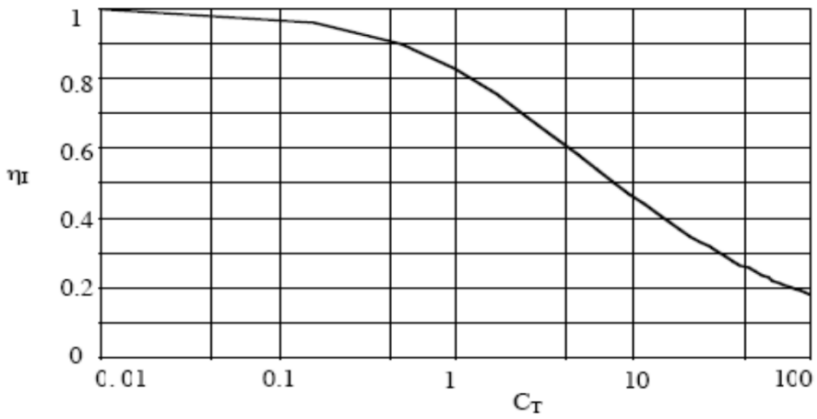

Figure 8 Efficiency of ideal propulsion unit as function of thrust loading coefficient [15]

1.3 Previous Studies

RANS based CFD tools have shown to be effective in hydrodynamic designs and they are used widely in design offices. They are seen efficient to develop concepts prior to model testing phase. In addition, they are favorable when optimal appendages are checked with wake field and power information as shown in [1], [16]. There are some studies that support to define accuracy of results in this thesis. Self-Propulsion is studied previously with an iterative coupled viscous/potential method, where free surface is modelled directly and an unsteady RANS method with sliding mesh, where wave making resistance is accounted for approximately. This study compared these methods to experimental data. Iterative method and RANS –method self-propulsion power estimates were within the range of 3 % and 0.6 % compared to experimental data, respectively. In addition, corresponding hull-propeller interaction coefficients were within the range of 3 % and 4 %, respectively as shown in the study [17]. These results were judged sufficiently high. From current solutions podded propulsion and hybrid propulsion concept with tunnel shaped aft body is seen

as an economical solution today. Shaft arrangements have a large effect on the wake field as shown in the study [1]. According to the study [18] indirect method called "numerical towing-tank technique" is recommended method to predict performance over the full scale simulation.

Unwanted boosting is studied in [19]. In this study, four-propulsion vessel was studied how the propulsion arrangement and hull affects the load change of propellers as in designed situation load is evenly distributed. Conclusion is that hull shape has the largest impact on the load change of propellers. In addition, pure interference of other propellers leads to about ten percentages of load change. Both have positive effect on the mid sided propeller and negative effect on side propellers.

Two different ways of modelling a propeller is studied in [20]: Actuator disk method and full RANS approach, where propeller is meshed geometrically. Actuator disk method is less power consuming method where propeller is represented by equivalent body force. Full RANS approach is more reliable method as there are no uncertainties related to body force modelling. Conclusion of the study is that body force method is significantly faster, however it overestimates induced velocity, which leads to a lower effective wake with higher thrust and torque.

In the research [2], it is discussed that higher efficiency in the propeller design leads to larger propeller that causes higher cavitation and hull pressure pulses. In this specific case, it is noted that cavitation is yet non erosive and hull pressure pulses are within the limits for cargo type of a ship.

In the study [18] of computational predictions, it is noted that following results (Table 1) are sufficient except for thrust deduction factor. The key point is the difference in percentages between the calculation and experimental value, which are CFD simulation and model test in this case.

Table 1 Results from study [18]

	Difference (%)
Thrust deduction factor (t)	-17.97
Wake fraction coefficnet (w)	-8.38
Hull efficiency η_H	1.08
Propeller open-water efficiency η_O	3.96
Effective power P_E	0.77
Delievered power P_D	-8.86

2 Methods

2.1 Research Setup

2.1.1 General

Research is done by step by step -process to minimize error during the process. Model tests are performed prior to this thesis (Figure 9). Efficiency of the new concept is analyzed and compared to current solutions through these model test reports to verificate its performance. Actuator disk model is benchmarked against open water curve in order to verificate its performance. CFD and Matlab simulation code are calibrated with model test in order to minimize error in modelling in CFD and Matlab simulation; therefore it is effortless to observe if these tools are able to model the different power divisions. CFD results and Matlab simulation results are compared to model tests to check how well these match together.

In general, there is no model tests done in early phase of the design, therefore 20 knot speed is used to check CFD performance when there is no model test performed for the calibration of the model. Matlab simulation code is used for 20 knots initial values for CFD. In addition, model tests are used to check predefined power divisions; however the most optimum power division is the most interesting one. Matlab simulation code was used to find the optimum curve for ideal power division for different speeds. Advance calculation point was calibrated for CFD in order to have right advance coefficient for the propeller. This ensures correct performance of the actuator disk to have the closest conditions as possible compared to model test environment.

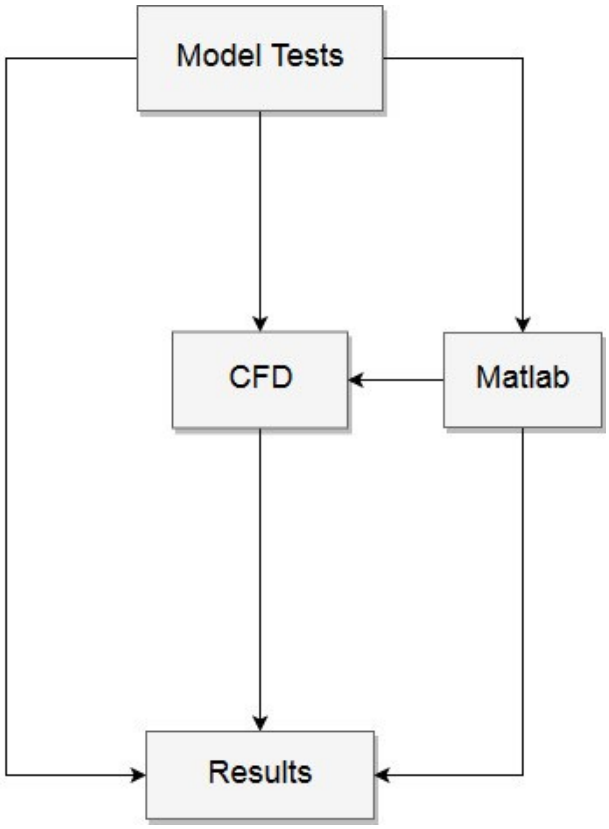

Figure 9 Principle of research setup

2.1.2 Calibrating the CFD Model

The basic idea to calibrate CFD model was to recreate model test environment with CFD. It was calibrated to have equivalent advance velocity with the model test results in different conditions. Open water curve was taken from the tests and rate of revolutions of the propeller units. Next step was to run CFD simulation with approximated advanced velocity calculation point. After first run advance coefficient values were compared with CFD and model tests. Next step is to rerun with an overestimated advanced velocity calculation point, therefore the correct point is between these two points. Assumed correct advance velocity calculation point is interpolated between obtained points (Figure 10). This is done for every speed, however not for different boosting situations, since point is velocity dependent.

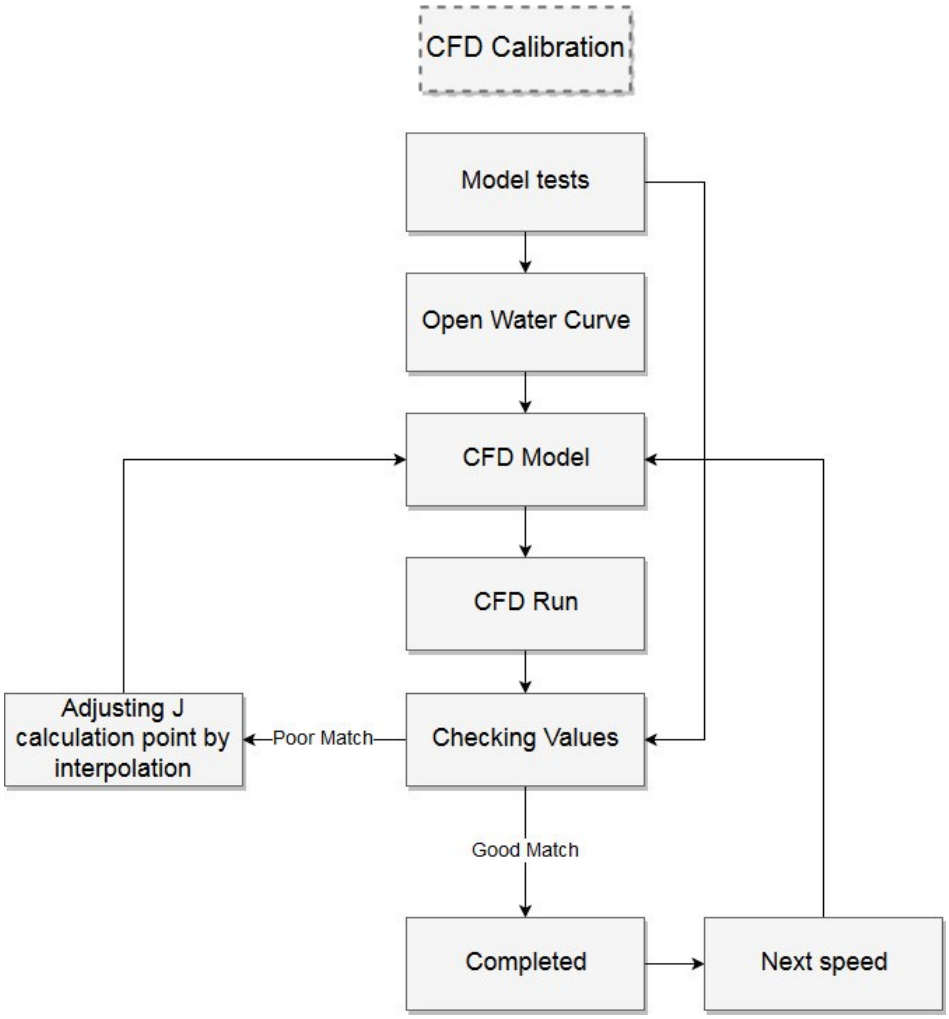

Figure 10 Calibration procedure of the CFD model

Shaft power was obtained by obtaining delivered power with KQ-method (2) as shown in the [21]. KQ-method is a simple tool to estimate power:

$$P_D = 2\pi n Q. \tag{2}$$

In this thesis it was used to compare power values of different methods.

2.1.3 Comparison

Comparison of the results is challenging. Model setup is significantly different between model test, CFD and Matlab simulation code. New factor of resistance correction factor was introduced to obtain rough estimate of other propulsion factors. This was done by performing bare hull CFD simulation without acting actuator disks. Obtained bare hull resistance was compared to model test appendage resistance to achieve rough estimate of appendage resistance in percentages. Comparing model test bare hull resistance to model test appendage resistance would be proper method in order to avoid errors between CFD and model tests. Unfortunately, bare hull resistance by model tests is not available. Factor was used to correct the resistance of the CFD simulations. In principle, the resistance correction factor was included to the resistance from CFD simulations to obtain rough estimate of appended hull resistance.

Thrust coefficient, advance coefficient, open water efficiency, resistance, viscous resistance and pressure resistance is taken from the model tests and according to these other model factors are calculated to be compared to CFD results. Factors are calculated from these values and CFD results such as: Thrust, advance coefficient in open water, advanced velocity, wake, corrected resistance, thrust deduction factor and hull efficiency (Figure 11).

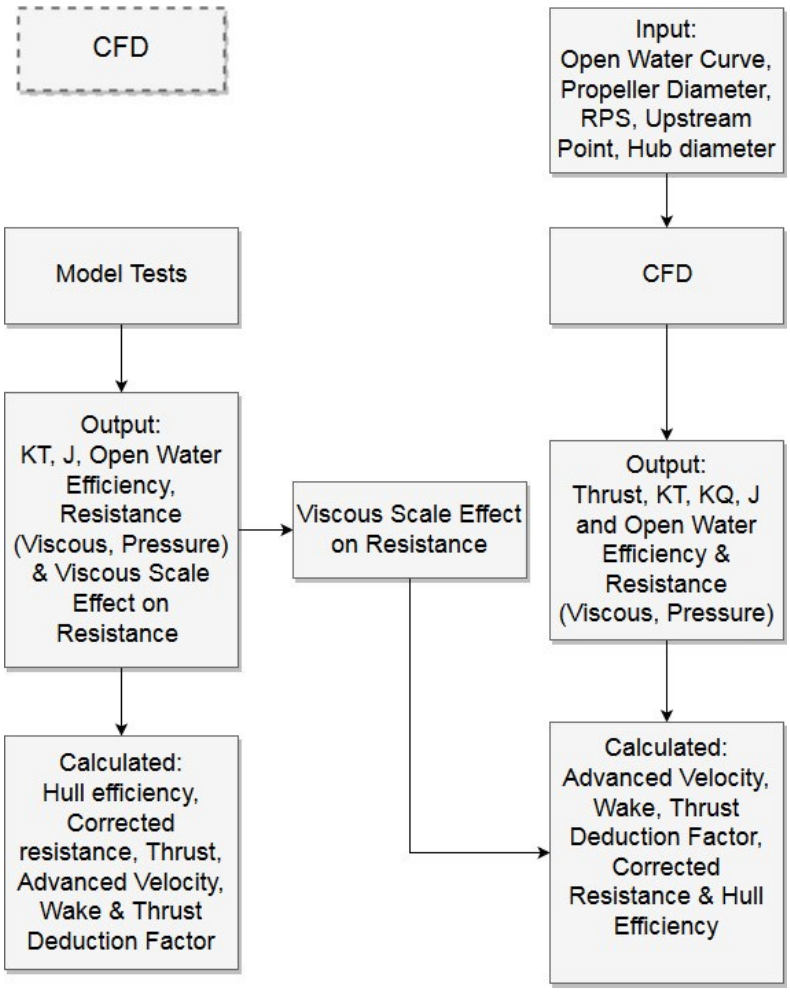

Figure 11 How CFD simulations are setupped with help of model test results

2.1.4 Matlab simulation

Matlab simulation code minimizes the total power of propellers to match the resistance that is calculated from effective power. Matlab simulation code (Appendix 1) was done by using model test reports. Information from open water tests, resistance test and propulsion test were used for estimating the best possible power combination for this specific case. However, most of these values can be estimated for a case without model test reports, even if it increases the error margin. This code uses in-built function of Matlab called fmincon as described in [22]. It is a nonlinear programming solver that finds the minimum of a problem specified by function, constraints and upper and lower limits.

Matlab simulation code can be used to estimate the most efficient power division combination. Inputs that are needed to execute the program are open water curves, educated estimation for effective power, diameters of propellers and velocity of the vessel. In addition, thrust deduction factor, advanced velocity of the propeller can be used as additional inputs to increase the accuracy. Simulation code needs an initial guess that starts the optimization method. In this case advance coefficients are used as the initial guess.

Matlab simulation code utilizes interior-point algorithm to solve the minimum of the function. In addition, it uses finite-differencing method to calculate the gradient and hessian of the objective function and constraint function.

2.2 Boosting

In the design condition propellers are loaded equally and they have one ideal velocity. Idea of boosting is to transfer power from less efficient propulsion units to more efficient propulsion unit to maximize power use in the most efficient way, when the resulted thrust remains the same.

This study uses propulsion arrangement of one large centerline propeller and two side pod units. The efficiency of every propeller unit is decreased when power divisions of design condition propellers are modified. For example, Figure 12 and Figure 13 present all three propellers in the aft. In the designed situation the point is on the top of the efficiency curve, however when power is increased advance coefficient value decreases, since RPM increases. This decreases the efficiency. Same principle applies to POD units but opposite direction, since total power remains the same. POD RPM decreases and advanced velocity coefficient value increases; this decreases the efficiency of the POD unit. Situation is not necessary the same when velocity changes, then boosting could be useful. Therefore propellers should be designed in a way that boosting situation is a design power division if velocity profile is roughly constant.

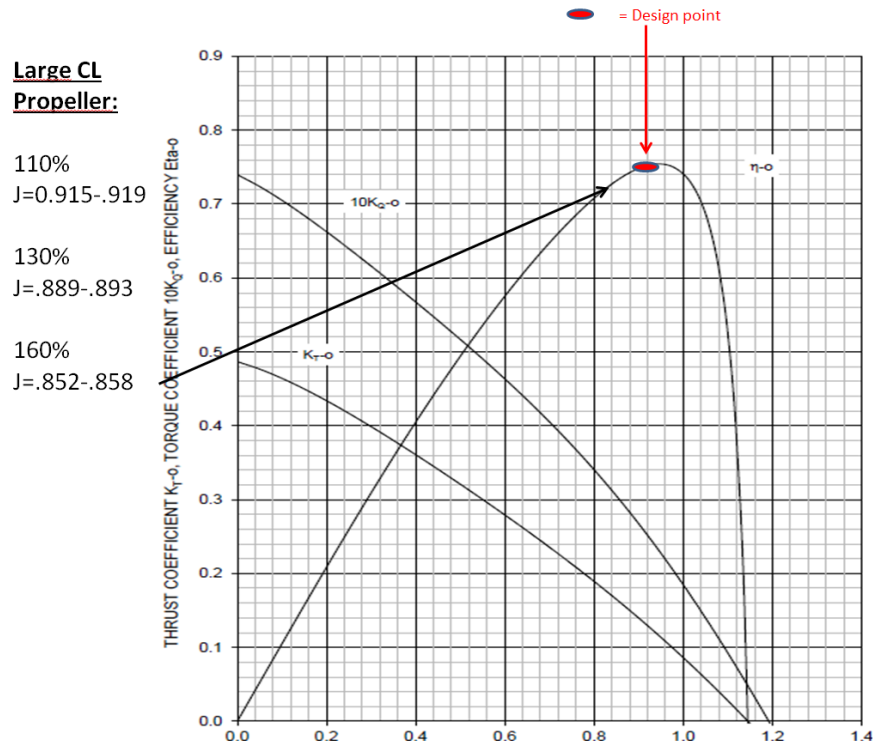

Figure 12 Open water curve for large centerline propeller

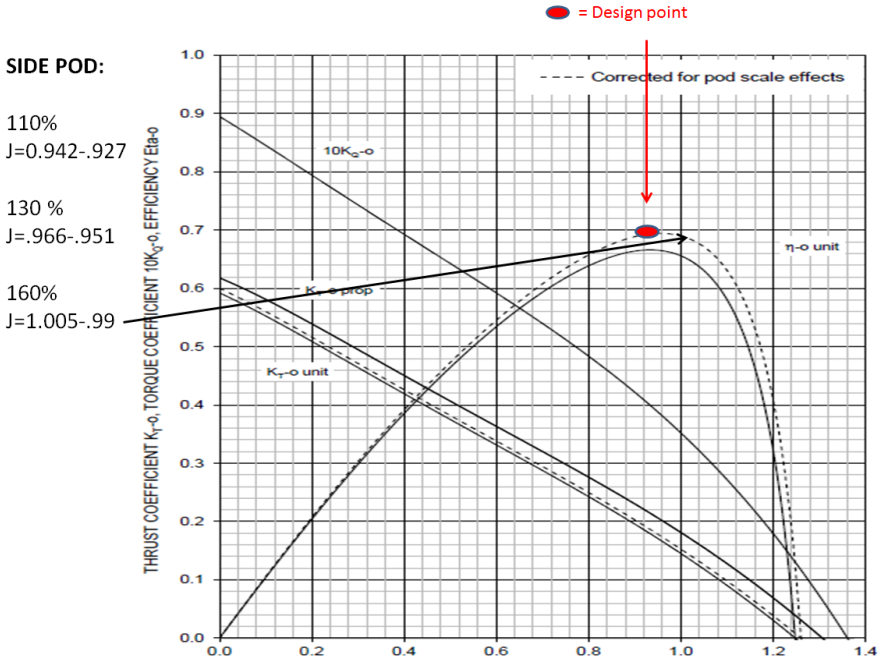

Figure 13 Open water curve for POD

2.2.1 Modelling Boosting

RPM is constantly changed during a propulsion test to set up different boosting situations in the boosting test in Marin model basin. For example, during the first run pod units have constant RPM, yet centerline propeller RPM is modified during the run. Boosting with CFD is done similarly than with model tests. Difference is that during one run RPM of all propulsion units can be changed.

If basic model test results are not available, the principle (Figure 14) is that Matlab simulation code provides target advanced coefficient values that are used to calibrate the advanced velocity calculation point as in (2.1.2). Different boosting situations can be simulated after calibrating by just changing the reference velocity which is diameter multiplied with rate of revolutions.

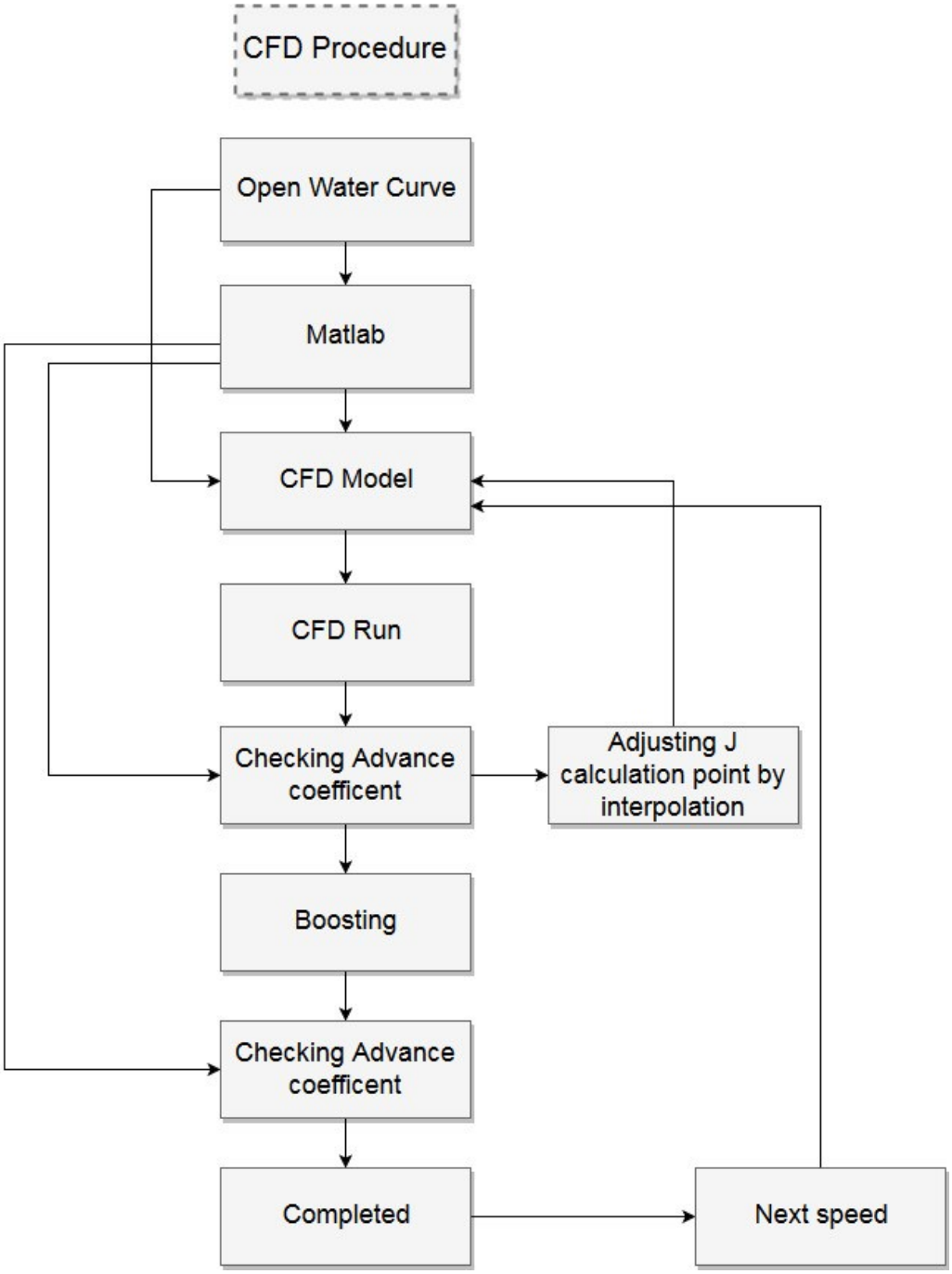

Figure 14 CFD simulation procedure without model tests

2.3 Propulsion

Boosting bases on the propulsion, that consists of resistance and open water characteristics of the propeller. Formulas used in propulsion section can be found in [21].

2.3.1 Open Water Characteristics

Open water characteristics describe performance of the propeller in the undisturbed flow. There are different dimensionless characteristics such as advanced coefficient (3), thrust coefficient (4) and torque coefficient (5):

$$J = \frac{V_a}{nD} \tag{3}$$

$$K_T = \frac{T}{\rho n^2 D^4} \tag{4}$$

$$K_Q = \frac{Q}{\rho n^2 D^5}. \tag{5}$$

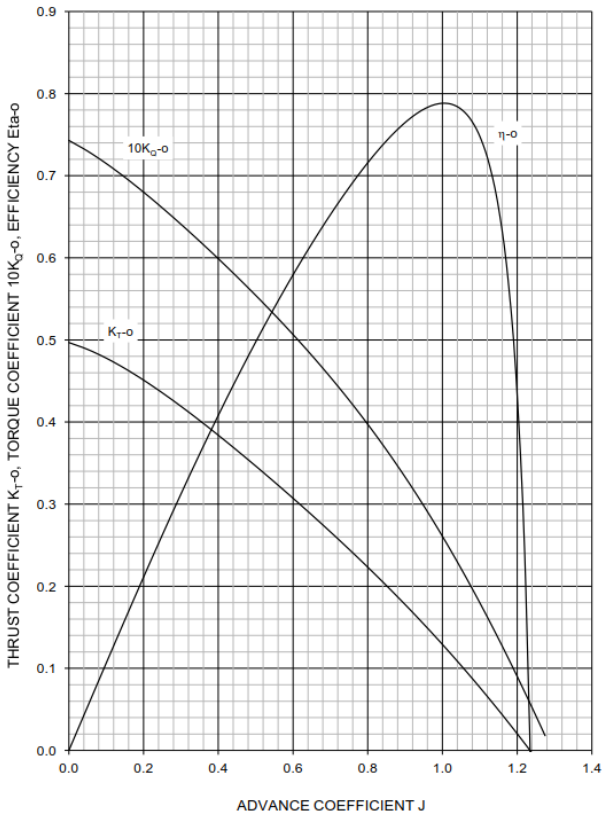

Figure 15 Example of the open water curve [12]

These coefficients are obtained from the open water model tests, CFD simulations or propeller design software and they are presented with the open water curve (Figure 15). These coefficients are used in the analysis of the propulsion tests and the estimation of the required power as torque coefficient is used to estimate required power, thrust coefficient is used to calculate the thrust and advance coefficient is used for the wake fraction coefficient.

There are different methods to model the propeller, such as momentum theory, lifting-line method, lifting-surface method, boundary element method and RANSE method. Momen-

tum theory is used, since it is the simplest and fastest of these methods as shown in the [23].

2.3.2 Momentum Theory

In this theory propeller is reduced to be an actuator disk that creates a pressure jump in the flow. The advantage of this theory is that it requires less computational power, since it is simpler than actual propeller model. However, momentum theory is not sufficient to be used to design propellers as rotative and viscous losses are not modelled, however it is sufficient to be used as propeller model in self-propulsion test as shown in the study [20].

2.3.3 Actuator Disk

Actuator disk is currently widely used as an option for direct propeller simulation is self-propulsion as shown in [18] and discussed in sea trial academy [24]. Actuator disk is using input of open water curve of the propellers. Actuator disk is fixed to its position. It does not follow the movement of the ship, when it is trimming or sinking. In this case, it is known that this specific model is rather stable with respect to trimming and heave (Figure 16).

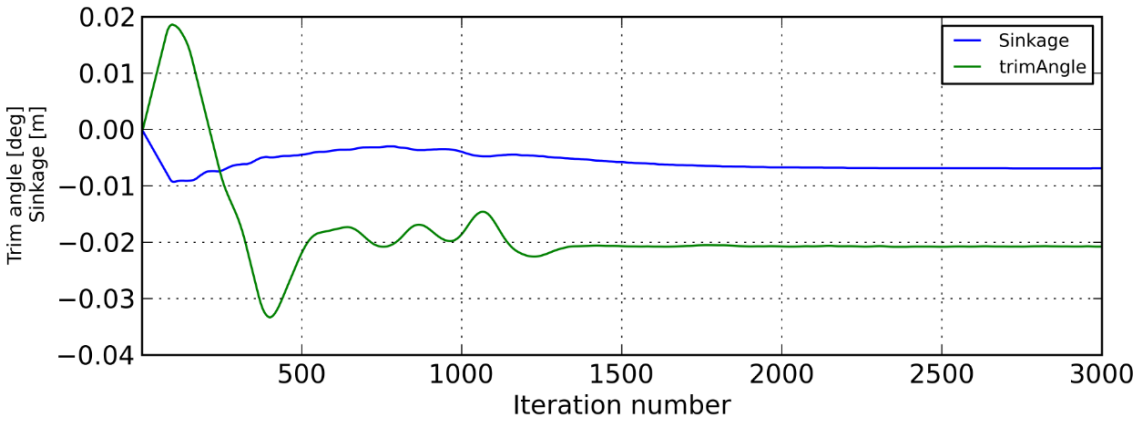

Figure 16 Trim angle and sinkage of the model

Actuator disk bases on the momentum equations. Body-force term is used to model the effects of a propeller without modelling the real propeller. These body forces represents body forces per unit volume normalized by $\rho U^2/L$, where U is reference velocity, that is in this case n*D, L is a reference length, which is D and ρ is the fluid density. In principle, there is no loading at the root or tip of the propeller as described in [25]. Body force with axial (6) and tangential components (7) are prescribed in the code:

$$f_{bx} = A_x r^* \sqrt{1 - r^*} \tag{6}$$

$$f_{b\theta} = A_\theta \frac{r^* \sqrt{1 - r^*}}{r^*(1 - r_h') + r_h'} \tag{7}$$

where

$$r = \sqrt{(y - Y_{PC})^2 + (z - Z_{PC})^2} \tag{8}$$

$$r^* = \frac{r' - r_h'}{1 - r_h'} \qquad r_h' = \frac{R_H}{R_P} \qquad r' = \frac{r}{R_P} \tag{9}$$

$$A_x = \frac{C_T}{\Delta}\frac{105}{16(4+3r_h')(1-r_h')} \tag{10}$$

$$A_\theta = \frac{K_Q}{\Delta J^2}\frac{105}{\pi(4+3r_h')(1-r_h')} \tag{11}$$

$$C_T = \frac{T}{\rho U^2 \pi D_P^2}. \tag{12}$$

R_P is the propeller radius, R_H is the hub radius, Δ is the actuator disk thickness and Y_{PC} and Z_{PC} defines the center of actuator disk. In the OpenFOAM K_T and K_Q are defined by the open water curve with help of advance coefficient which is calculated with advanced velocity calculation point and R_P, R_H, n and center of the actuator disk are defined by the user. Variable r (8) is the normalized distance to propeller in the propeller plane. Coefficient r* (9) is the dimensionless distance between hub and tip of the propeller. In practice, when r* is zero point is at the hub and if it is 1, point is in the tip of the propeller. K_T, K_Q and J are calculated as in section 2.3.1. C_T is thrust coefficient (12) other two coefficients are A_x (10) and A_θ (11) and these are solved with usage of open water curve that are inputted to the OpenFOAM, therefore body forces can be solved and thus the thrust and torque.

As derived, these forces are defined over an "actuator disk" with volume defined by R_P, R_H and Δ. Integration of the body forces over this analytical volume exactly recovers the prescribed thrust (13) and torque (14):

$$T = \rho L^2 U^2 \iiint_A f_{bx} dA \tag{13}$$

$$Q = \rho L^3 U^2 \iiint_A r f_{b\theta} dA \tag{14}$$

where

$$dA = 2\pi r \Delta dr. \tag{15}$$

2.3.4 Resistance

There are numerous reasons to have resistance as low as possible. Higher resistance means higher propulsion load, higher environmental impact, higher operational cost and more weight due to larger engines.

Total resistance of the ship can be divided in to two main components (Figure 17): friction resistance and pressure resistance. More detailed decomposition of resistance can be found in [23]. Friction resistance is often described as a function of Reynolds number and pressure resistance is often described as a function of Froude's number. Larger wetted surface means higher friction resistance. Pressure resistance is related to wave formation, so it is more dependent on the curvatures of the hull.

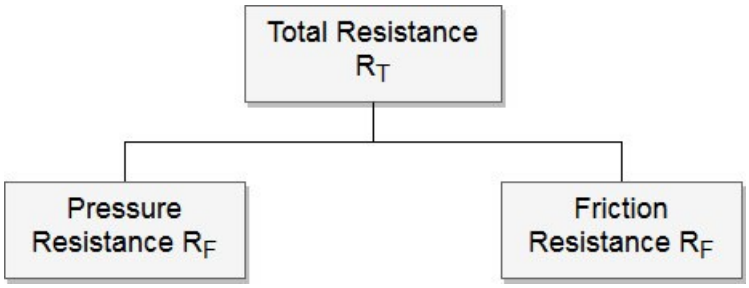

Figure 17 Simplified decomposition of resistance

Speed of the vessel determines which one of resistance components dominates in total resistance. In principle, lower Froude number means that friction resistance is dominating and higher Froude number that pressure resistance dominates for displacement hulls.

Appendages modify the flow field that has an effect on pressure resistance. For example, holes in the hull, such as bow thrusters, stabilizer fin recesses modify flow and have effect on pressure resistance, where appendages such as pod housings, shafts have higher effect on viscous resistance. These appendages are rather difficult subject in the model scale since flow is mainly dominated by viscous forces which require Reynolds similarity. Model tests can be performed with geometrically properly scaled appendages, however scaling to full scale requires carefulness as described in [23].

2.3.5 Wake

Propeller is acting in a wake that hull body forms. Hull disturbs the water flow, therefore propeller is acting in non-uniform wave field. In general, the water around the stern acquires a forward motion in the equivalent direction as the ship, which means that advanced velocity of the propeller is lower than speed of the ship. This phenomenon is called as a wake. Wake is not uniform in the propeller plane due to hull shape. Centerline propeller is more aft in this new concept; therefore, wake should not be as effective as it would be in normal position since there is time for the flow to stabilize.

Wake fraction coefficient (16) is the ratio of the difference of the advanced velocity and the velocity of the vessel and the velocity of the vessel, therefore it is basically a difference between velocity in undisturbed flow compared to disturbed flow that hull forms in front of the propeller:

$$w = \frac{V - V_A}{V}. \tag{16}$$

2.3.6 Thrust Deduction Factor

Propeller accelerates the flow at ship stern, which means that pressure decreases in the aft body, therefore inviscid resistance increases. This phenomenon is called as thrust deduction as described in [15]. This is usually assumed to be the same for model and the ship, even if the friction component introduces a certain scale effect as indicated in [23]. Clearance of the propeller has a large effect on the thrust deduction factor. Large clearance lowers the thrust deduction factor, which is one reason for restrictions for propeller diameter when it is under the hull.

Thrust deduction factor indicates how propeller changes the flow conditions for the hull. Thrust deduction factor is a ratio between difference of the total thrust and the total resistance in the calm water and the total thrust of the vessel (17)

$$t = \frac{T - R_T}{T}. \tag{17}$$

In principle it indicates, how much larger resistance of the hull is with acting propulsion compared to situation without propulsion.

2.3.7 Efficiencies

The differences between different power concepts are presented in the Figure 18.

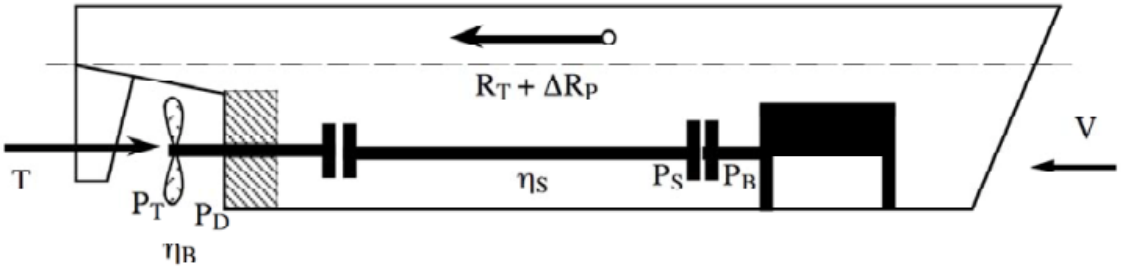

Figure 18 Principle picture from the different power measures and efficiencies [15]

The hull efficiency (18) is defined as ratio between the effective power ($P_E = R_T \times V$) and the thrust power, which the propeller deliverers to the water ($P_T = T \times V$):

$$\eta_H = \frac{P_E}{P_T} = \frac{1 - t}{1 - w}. \tag{18}$$

Range for the hull efficiency values are usually between 0.95 - 1.4. It is dependent on the propulsion arrangement and shape of the ship as hull efficiency is dependent on the thrust deduction and wake. For one propeller, it is usually higher than with twin propellers as indicated in [21].

Open water efficiency (19) describes how well propeller works in homogenous wake field i.e. when hull is not disturbing wake field in front of the propeller:

$$\eta_0 = \frac{K_T J}{K_Q 2\pi}. \tag{19}$$

Open water efficiency can vary from 0.35 to close to 0.8.

Flow into propeller is never homogenous. There is always some rotational flow in to propeller area; therefore there is relative rotative efficiency. It is usually between 1.0 and 1.07 for single propeller ships and for twin propeller ships without twin-skeg solution it will be less down to 0.98 as indicated in [21].

Propeller efficiency (20) is the ratio between the thrust power and delivered power, therefore it is combined factor of open water and relative rotative efficiency:

$$\eta_B = \frac{P_T}{P_D} = \eta_0 \times \eta_R. \tag{20}$$

Propulsive efficiency is determined as a ratio of effective power and power delivered to propeller. Delivered power is the minimum required power delivered to the propeller that is needed for the ship to sail at constant speed and. The power required to have this speed is the effective power.

Shaft efficiency (21) depends on the alignment and lubrication of the shaft bearings, and on the reduction gear if there is one installed. It is the ratio between delivered power and brake power that is delivered by the engine:

$$\eta_S = \frac{P_D}{P_B}. \tag{21}$$

Total efficiency (22) is the ratio between the effective power that is needed to motion the vessel and the power that is got out from the main engine:

$$\eta_T = \frac{P_E}{P_B}. \tag{22}$$

Main focus can be on the propulsion efficiency rather than total efficiency when propulsion is under review as stated in [21].

2.4 Model tests

Model tests are considered as the most reliable way to do resistance and propulsion tests. CFD calculations are gaining more room every year in ship design as it is easier and faster than model tests. CFD have already replaced some of model tests such as defining the orientation of some appendages as bilge keels and shaft supports as discussed with Head of Hydrodynamics of the shipyard in Turku [13].

2.4.1 General

Model tests are usually performed in towing tanks, where water is still, and the model is towed by a carriage. Special wires, which are attached to end of the model (Figure 19), keep the model in right course, however model is free to trim and heave. Other options to do resistance and self-propulsion model tests are in depressurized tank, where air pressure is reduced. It gives possibility to test ships in most realistic but scaled operational conditions. In addition, there are cavitation tunnel for propellers, where cavitation behavior can be predicted.

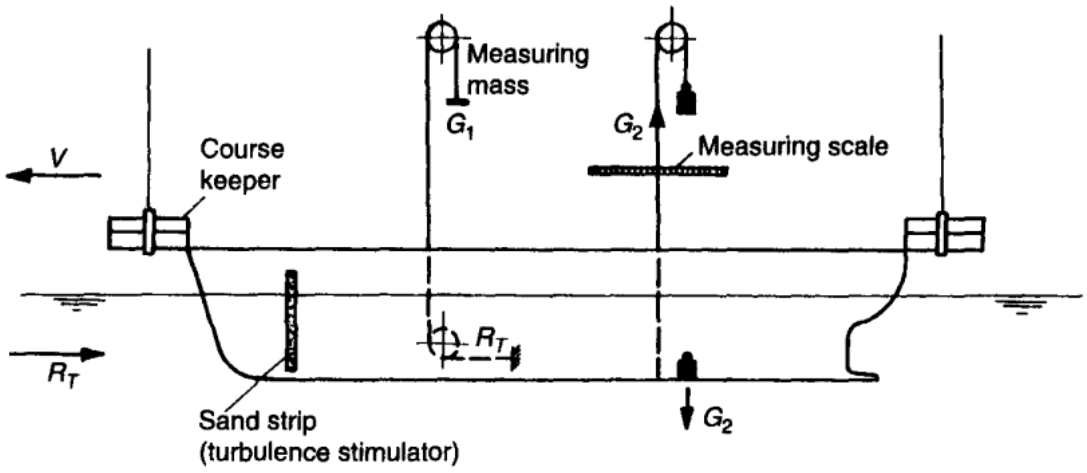

Figure 19 Schematic picture of the model [23]

Viscous effects are larger in model scale; therefore, model needs to be large as possible to have minimum viscous effects. However, there are restrictions for model size, since water is restricted in the basin and certain speed needs to be achieved with carriage. Model basins use a blockage correction factor on resistance, due to reasons that water basin is restricted. In addition, strength issues need to be considered.

The basic test procedure (Figure 20) is to do resistance test for the hull, open water test for the propellers and propulsion test.

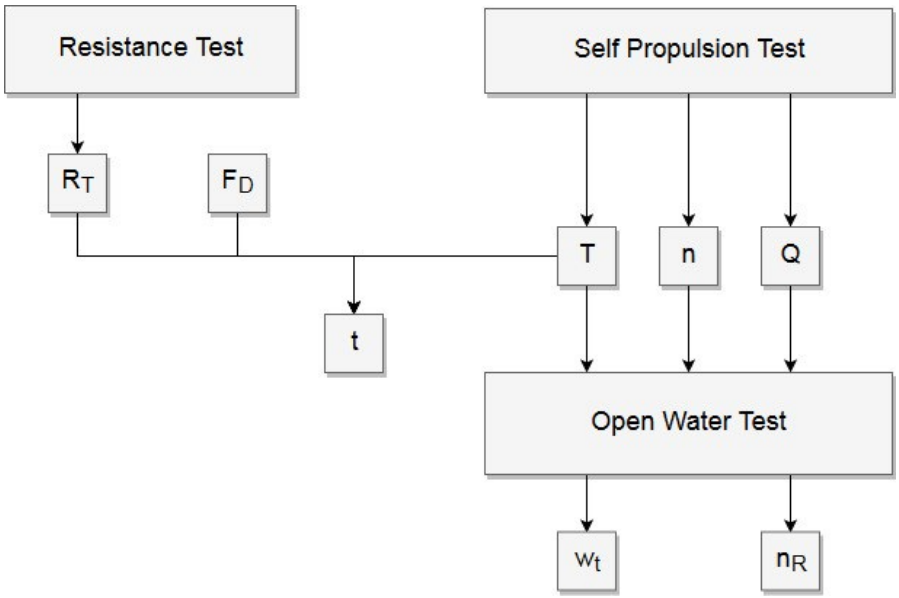

Figure 20 Basic test procedure

Open water tests are used to find out hydrodynamic characteristics of the propeller in different conditions. Tests are performed in uniform flow revolutions are often assumed as constant, where advance velocity varies (V_a). This is done by having more speed with carriage. This is how advance ratio (J) is modified. In addition, thrust (T) and torque (Q) are measured from the propeller.

Resistance test is used to determine the resistance of the model. This is done without acting propeller and it can be done for both naked hull and hull with appendages. Results of the test are later used to determine thrust deduction factor. Propulsion test are performed with acting propeller and other relevant appendages.

Tests are done according to Froude scaling, which means that Froude number (23) is constant:

$$F_n = \frac{V}{\sqrt{gL}}. \tag{23}$$

As Froude number is dimensionless number it is same for model and full-scale ship (24) (25):

$$F_{n_M} = F_{n_S} \tag{24}$$

$$\frac{V_M}{\sqrt{gL_M}} = \frac{V_S}{\sqrt{gL_S}}. \tag{25}$$

Scaling ratio is ratio of the length of the ship and model (26):

$$\lambda = \frac{L_S}{L_M}. \tag{26}$$

When formula (25) is modified in a way that speed of the model is on the left side of the formula and scaling ratio (26) is added, therefore a scaling formula (27) is obtained for the velocity that is used in the model tests:

$$V_M = \frac{V_S}{\sqrt{\lambda}}. \tag{27}$$

Model speed is lower than in full scale with Froude's scaling. However, when Reynold's number is kept as constant and same procedure is done as for Froude's number (28, 29), model speed (30) is larger than full scale, which is a problem, and therefore Froude's scaling is used:

$$R_{n_M} = R_{n_S} \tag{28}$$

$$\frac{V_M L_M}{\nu_M} = \frac{V_S L_S}{\nu_S} \tag{29}$$

$$V_M = V_S \lambda. \tag{30}$$

Viscous effects are over dimensioned in the model scale with Froude scaling. Viscous effects needs to take into account when results are scaled from model scale to full scale. There are numerous of scaling methods. ITTC-78 method with Grigson's friction line is used since Grigson's friction line is used in model tests that this thesis uses as a reference.

2.4.2 ITTC-78 Method

Resistance of model R_{TM} is obtained from the resistance tests. Total model scale coefficient (31) is obtained by forming total resistance non-dimensional:

$$C_{TM} = \frac{R_{TM}}{\frac{1}{2}\rho_M V_M^2 S_M}. \tag{31}$$

Model frictional resistance coefficient C_{FM} is calculated with Grigson's method, since it is used in the model tests. ITTC coefficient (33) is multiplied with Grigson's multiplier (34,35,36) in order to obtain Grigson's line coefficient (32) as described in [26]:

$$C_{FGrigson} = g(\gamma) C_{FITTC} \tag{32}$$

where

$$C_{FMITTC} = \frac{0.075}{\left(\log_{10} R_{n_M} - 2\right)^2} \tag{33}$$

$$g(\gamma) = 0.9335 + 0.147(\gamma - 6.3)^2 - 0.071(\gamma - 6.3)^3 \tag{34}$$

for $1.5 \times 10^6 < R_N < 20.0 \times 10^6$

and

$$g(\gamma) = 1.0096 + 0.0456(\gamma - 7.3) - 0.013944(\gamma - 7.3)^2 + 0.0019444(\gamma - 7.3)^3 \tag{35}$$

for $R_N > 20.0 \times 10^6$

where

$$\gamma = \log_{10} R_n. \tag{36}$$

Residual coefficient (37) is the same for model and ship since it is dependent on the Froude's number. In this case, same form factor is used as in model tests; however it can be obtained with Prohaska's method as described in ITTC -report [27]:

$$C_R = C_{TM} - (1 + k) C_{FM}. \tag{37}$$

Friction coefficient (38) is calculated for a ship:

$$C_{FS} = \frac{0.075}{\left(\log_{10} R_{n_S} - 2\right)^2}. \tag{38}$$

Total resistance coefficient (39) is obtained by combining coefficients including correlation allowance:

$$C_{TS} = (1 + k) C_{FS} + C_R + C_A. \tag{39}$$

Total resistance coefficient is multiplied with density, speed and wetted surface area to modify values from unidimensional and effective power is product of speed and total resistance (40):

$$R_{TS} = C_{TS}\frac{1}{2}\rho_S V_S^2 S_S. \quad (40)$$

Effective power (41) is the obtained by multiplying speed and the resistance of the vessel:

$$P_E = R_{TS} V_S. \quad (41)$$

2.4.3 Model Testing in MARIN

Propulsions tests were conducted in the Deep-Water Towing Tank in the MARIN model basin facility in the Wageningen, Netherlands. Dimensions of the tank are 250 x 10.5 x 5.5 in meters in length, width and depth, respectively. A semi-captive test setup was used for the tests. During the open water tests and the propulsion test, MARIN measured the thrust and torque delivered by the propeller as discussed in the model test report [12].

MARIN uses their own method to correct pod open water characteristics for pod housing scale effects. This method is called as POD-U method. It considers the difference in hydrodynamic characteristics between various types of pod housings. The method leads to scale effect corrections, which depend on the speed and loading of the propeller. The open water characteristics have also been corrected for scale effects on the propeller blade friction. The corrections are applied to K_T and K_Q as explained in [12].

Marin uses theirs 3-D extrapolation method for resistance and propulsion. This is bases on so-called form factor concept. In this method, Grigson formula is used for model-ship correlation incorporating a form factor and a model-ship correlation allowance C_A, that includes the effects of the still-air drag of the wind exposed ship and superstructure size are included as well. In addition, resistance from bilge keels is included in the C_A value as they are not fitted in the model. The form factor 1+k represents the ratio of the viscous to the frictional resistance and is based on resistance measurements at low speeds and is verified with statistical data and with a CFD calculation as explained in [12].

2.5 CFD Modelling

CFD is used to reproduce numerically the 3D flow around the vessel. It gives opportunity to obtain key information about the model or full-scale ship without doing expensive model tests. CFD simulations are an efficient way to study concepts or ships in early stages of the design and help to predict the performance of the ship. There are numerous amounts of CFD programs available. OpenFOAM software is used in this thesis.

OpenFOAM is primarily a C++ toolbox for the customization and extension of numerical solvers for continuum mechanics problems, including computational fluid dynamics. It has a lot of prewritten solvers that can be used to a wide range of problems. In addition, software includes a plugin for visualization of solution data and meshes with ParaView.

There are different ways to divide CFD methods into different groups. One of the common divisions is between inviscid and viscous methods. Inviscid methods neglects the viscous

forces and therefore are not sufficient for modelling stern flows as viscous effects dominates in the stern area due to boundary layer as discussed in the [28]. Inviscid methods use significantly less computer power as viscous methods. Viscous method is used since stern area of the vessel is under the focus in this research.

CFD is performed with a simplified simulation setup to have minimum computational power, therefore hull does not have appendages, propeller is modelled as an actuator disk and only half of the hull is used. Model test reports contains the raw model values and scaled full scale values, therefore CFD values were scaled according to same values (Table 2) as in model tests. In addition, one extra scaling factor was introduced; resistance correction factor, due to lack of appendages in CFD simulation.

Table 2 Used calculation coefficients for scaling

	Value	Unit
1+k	1.125	-
C_A	0.00028	-
Density	1025.9	kg/m^3
Resistance correction factor	10.77	%
kinematic viscosity	1.19E-06	m^2/s

CFD is used as a tool, therefore the most relevant aspects of the CFD simulations is briefly discussed and more detailed theory behind these concepts and equations can be found in [29].

2.5.1 Base equations of the CFD

The foundation of CFD bases on two formulas. The Navier-Stokes equations (42) and the continuity equation (43) for incompressible flows together describe all real flow physics for ship flows. The Navier-Stokes equations bases on the Newton's Second Law and it is expression for fluids, stating that mass times the acceleration of fluid particles is proportional to the forces acting on them.

With Einstein summation rule, these equations can be written in compact form:

$$\frac{\partial u_i}{\partial t} + u_j \frac{\partial u_i}{\partial x_j} = -\frac{1}{p}\frac{\partial p}{\partial x_i} + F_i + \nu \frac{\partial^2 u_i}{\partial x_j \partial x_j} \tag{42}$$

$$\frac{\partial u_i}{\partial x_i} = 0. \tag{43}$$

These formulas can form the appropriate mathematical model for viscous fluid flows, however it is practically impossible to solve these equations for ship flow, therefore RANS equations are formed, which are obtained by time-averaging.

2.5.2 Boundary Conditions

The Navier-Stokes equations may be mathematically classified as second order, elliptical partial differential equations. These kinds of equations requires conditions on all boundaries of the computational domain, therefore boundary conditions are necessary in CFD simulations. Boundary conditions for the simulation can be seen in the Table 3.

Table 3 Boundary conditions of the mesh of the simulation setup

The boundary	p_rgh	U	k	omega	nut	pointDisplacement	alpha.water
atmosphere	totalPressure	pressureInletOutletVelocity	inletOutlet	inletOutlet	zeroGradient	fixedValue	inletOutlet
inletWater	fixedFluxPressure	fixedValue	fixedValue	fixedValue	calculated	fixedValue	fixedValue
inletAir	fixedFluxPressure	fixedValue	fixedValue	fixedValue	calculated	fixedValue	fixedValue
outlet	zeroGradient	outletPhaseMeanVelocity	inletOutlet	inletOutlet	zeroGradient	fixedValue	variableHeightFlowRate
hull	fixedFluxPressure	movingWallVelocity	kqRWallFunction	omegaWallFunction	nutUSpaldingWallFunction	calculated	zeroGradient
hullUp	fixedFluxPressure	movingWallVelocity	kqRWallFunction	omegaWallFunction	nutUSpaldingWallFunction	calculated	zeroGradient
cut	slip	slip	slip	slip	slip	calculated	slip

2.5.3 RANS Equations

RANS methods are sufficient in power prediction as widely indicated in [1], [18], [20], [23]. RANS have principal problems of modeling the turbulence. This problem is able to be avoided with other types of methods can be used such as Large Eddy Simulation or Direct Numerical Simulation. In LES methods turbulence of the flow is solved in full scale; however it is modelled in smaller scale. LES has higher accuracy in full turbulent cases, however boundary layer is still solved with RANS methods and it consumes higher amount of computational power. DNS methods solves full spectrum of the turbulence, however there is no practical solutions yet.

RANS equations (44, 45) are formed by time-averaging the incompressible continuity equation and the Navier-Stokes equations, however continuity equation is linear, therefore all turbulent contributions will disappear and the equation looks as before, but with the instantaneous velocities replaced by the mean values:

$$\frac{\partial \overline{u_\iota}}{\partial x_i} = 0 \tag{44}$$

$$\frac{\partial \overline{u_\iota}}{\partial t} + \frac{\partial}{\partial x_j}\left(\overline{u_j}\,\overline{u_\iota}\right) = -\frac{1}{p}\frac{\partial \bar{p}}{\partial x_i} + F_i + \frac{1}{\rho}\frac{\partial}{\partial x_j}(\sigma_{ji} + R_{ji}) \tag{45}$$

Where

$$R_{ji} = R_{ij} = -p\overline{u_\iota' u_j'}. \tag{46}$$

There are no turbulent fluctuations in this RANS equation, however Reynolds Stress (46) is introduced, and that needs to be modelled. It is a correlation between two fluctuating velocity components. Reynolds stress is symmetric and contains six independent components. A turbulence model is required to compute these.

2.5.4 Turbulence Modelling

There are different types of turbulence models such as zero-equation models, one-equation models, two-equation models, algebraic stress models and Reynolds stress models. The basis for first three models is the Boussinesq eddy viscosity assumption.

Boussinesq eddy viscosity assumption assumes that Reynolds stresses can be computed from the rate of strain tensor in the same way as the viscous stresses. The only difference is that the molecular viscosity is replaced by a turbulent equivalent, because viscous stresses arise from molecular mixing.

Two-equation models are the most common of all turbulence models. In this thesis k – ωSST model is used and it is widely used in engineering and seen as sufficient method as shown in the [30]. This model is a two-equation eddy-viscosity model and in this model, an equation for the specific dissipation rate (47) is solved:

$$\omega = \frac{\varepsilon}{k}. \tag{47}$$

Where k is the turbulent kinetic energy per unit mass and ε is rate of dissipation. K – ω model has been show as superior performance when predicting ship flows, as compared to k - ε model as discussed in [29]. The use of k- ω in the inner parts of the boundary layer form the model directly usable all the way down to the wall through viscous sub-layer, therefore SST k- ω can be used as low Reynolds turbulence model without any extra damping functions. The SST formulation also switches to a k- ε behavior in the free-stream and thereby avoids the common k- ω problem that the model is too sensitive to the inlet free-stream turbulence properties. It has satisfying behavior in adverse pressure gradients and separating flow, however it produces a bit too large turbulence levels in regions with large normal strain, like stagnation regions and regions with strong acceleration, however it is smaller problem than with normal k- ε model. Turbulence fluctuation is modelled as kinetic energy in two-equation models.

In general wake fields are sensitive to the turbulence model used and to grid density, but can be predicted fairly accurately using today's preferred turbulence models such as SST versions and a grid of a few million grid points for a bare-hull case.

However, some mature turbulence models such as k- ε are only valid in the area of turbulence fully developed; therefore they do not perform well in the area close to wall. There are two different ways to avoid this problem. First is to integrate the turbulence to the wall and another way is to use wall functions.

2.5.5 Near-Wall Modelling

Wall functions are empirical equations used to satisfy the physics of the flow in the near wall region. Wall functions are used to link the inner region between the wall and the turbulence fully developed region.

KqRWallFunction is used in this thesis for hull in OpenFOAM. It provides Neumann boundary, which means that one prescribes the gradient normal to the boundary of a variable at the boundary. It provides a pure zero-gradient boundary condition. There is omegaWallFunction for the dissipation ratio of turbulence and nutSpaldingWallFunction for tur-

bulent viscosity. In this case turbulent viscosity is calculated from speed not from kinetic energy, since bow of the hull has turbulators to form turbulent boundary layer almost from the bow, otherwise flow would be laminar at the bow and viscous resistance would be underestimated.

2.5.6 Free Surface Model

There are different methods to capture the free surface. Fully viscous solution is used in this thesis. To obtain the full free-surface/viscous flow interaction, the boundary conditions need to be considered in the viscous flow method. Kinematic condition ensures that there is no flow through the surface and dynamic conditions. In addition, dynamic conditions are expressed in tangential and normal directions. Often, viscous stresses and surface tension are neglected.

There are two principally different ways of treating the free surface in RANS methods: interface tracking methods and interface capturing methods. In the interface tracking methods, numerical grid is fitted to the surface and updated in each iteration or time step when the surface changes its shape. The kinematic and dynamic boundary conditions are applied on the surface and the flow is computed only in the water. In the interface capturing methods, the grid is fixed and location of the free surface in the grid is computed in every iteration or time step. The flow may be computed in both air and water, in which case the surface is just and internal boundary where viscosity and density change in a region as thin as possible, but where no boundary conditions are applied. Alternatively the flow maybe computed only in the water, in which case the boundary conditions are used.

Three different CFD codes were tested for free surface model in [16]: PARNASSOS a structured multiblock RANS solver with an interface tracking method, ISIS-CFD an unstructured face-based finite-volume solver that computes free-surface flow with a surface capturing approach without reconstruction, using compressive discretization schemes and SURF an unstructured finite-volume solver with a level set discretization of the free surface. ISIS-CFD is the closest setup compared to method in this thesis. Only ISIS-CFD of these three methods is able to simulate the dynamic ship movement to its equilibrium position as studied in [16].

The Volume of Fluid (VOF) method is used in this thesis, which is an interface capturing method. It is the most well-known method and it is a standard for general free-surface flow problems as indicated in [31]. In the VOF method, a transport equation (48) is solved for the void fraction c:

$$\frac{\partial c}{\partial t} + \frac{\partial}{\partial x_i}(u_i c) = 0. \tag{48}$$

If c is 1 it indicates that cell is fully contained with water and when it is 0 it is contained with air. Usually the surface is taken as c = 0.5. Term c is initialized at time t = 0 and computed at every time step in connection with the other transport equations.

2.5.7 Pressure-Velocity Coupling

RANS methods are formed with momentum equations, continuity equation a set of equations for turbulent quantities, however there is no explicit equation for pressure, but the pressure gradient in the RANS equation drives the velocity and the velocity has to satisfy

the continuity equation, so there is an indirect coupling between the pressure distribution and the continuity equation. In large class of CFD methods, this link is used to derive an equation for the pressure or for the pressure correction.

In this thesis, PIMPLE algorithm is used to solve pressure-velocity coupling in iterative way. It is a combination of PISO and SIMPLE. The best way to think about the PIMPLE algorithm is to imagine it as a SIMPLE algorithm for every time step, where outer correctors are the iterations, and once converged will move on to the next time step until the solution is complete. Better stability is obtained from PIMPLE over PISO for this reason, especially when dealing with large time steps where the maximum Courant number may consistently be above 1 or when the nature of the solution is inherently unstable.

For calculations Local Time-Stepping (LTS) is used. It is steady state calculation in practice. In this method time step is manipulated for each individual cell in the mesh, making it as high as possible to enable the simulation to reach steady-state quickly.

2.5.8 Grid

Numerical methods require a grid on which the continuous equations can be discretized. The whole computational domain must be covered by the grid and in the discretized equations; values of the dependent variables will be computed at the grid nodes. There are two main types of grids: structured and unstructured. In both cases, the entire grid may consist of only one block or it may be divided into two or more grid blocks. For the multi block grids, combinations of structured and unstructured block may be used as well.

The advantage of the structured grids is that they are computationally efficient. The disadvantage is that it is very difficult to represent complex boundaries. The major advantage of unstructured grids is flexibility. It is considerably easier to fit an unstructured grid to a complex boundary. In addition, the waste of cells in bands where a large density is not required is avoided. The disadvantage is the irregular data structure. The connectivity between the cells as well as their location has to be stored and the solution matric loses its diagonal structure, which increases the computational effort. Another disadvantage is the larger numerical diffusion associated with this type of a grid.

In this study, the mesh is performed earlier during resistance CFD simulations in the company; therefore it does not get too much focus in this study. Basic information of the mesh can be found in the Table 4.

Table 4 Qualities of the mesh of simulation setup

Patch	Faces	Points	Cell amount	Overall domain boundary box		
atmosphere	504	559		x	-40.8419	27.2279
inletWater	546	706		y	0	20.421
inletAir	309	346		z	-20.421	4.2232
outlet	792	871				
bottom	504	559				
side	25830	27316				
midplane	2772	2881				
hull	59407	66584				
cut	13244	13995				
Actuator disk POD			6887			
Actuator disk MID			7382			
Total			4491981			

Mesh of the simulation is in the figures: Figure 21, Figure 22 and Figure 23. Figure 21 show the mesh at the design water line. Grid is rather fine and triangle shape. This is due to kelvin wave pattern that is formed by the ship.

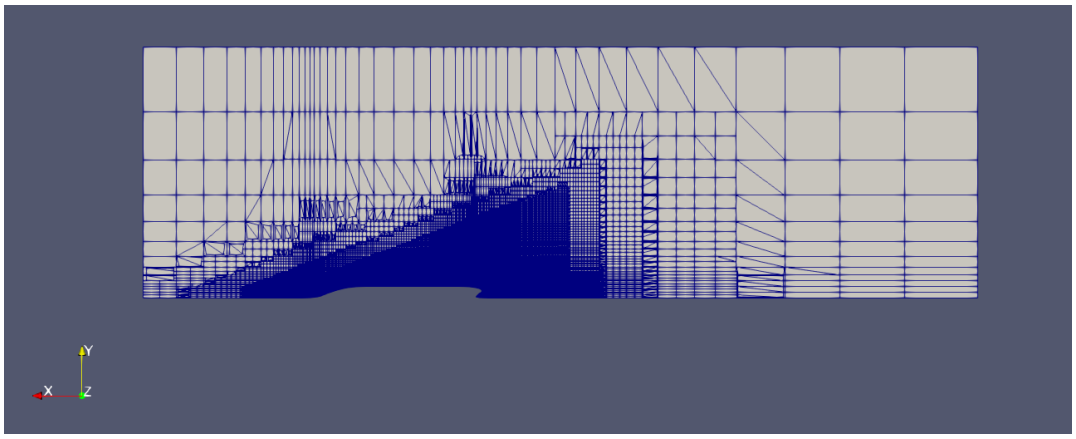

Figure 21 Design waterline mesh of the box

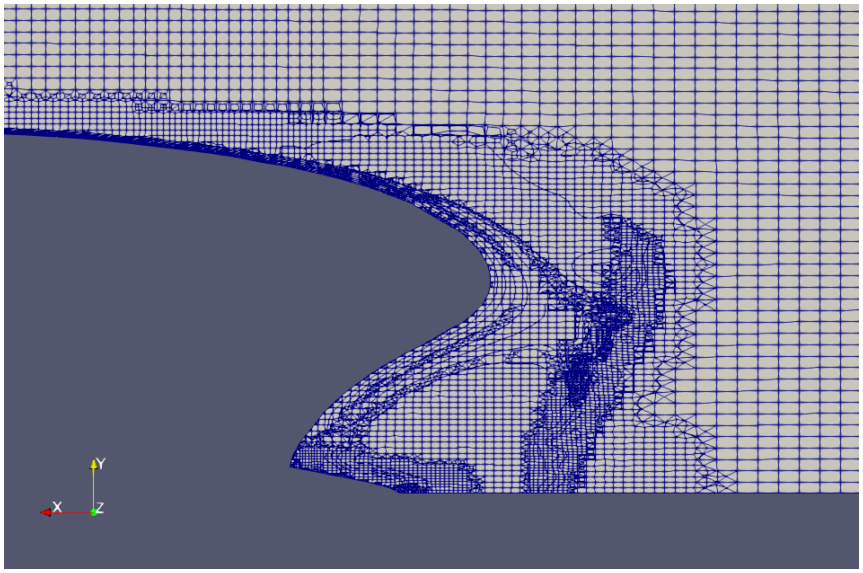

Figure 22 Aft mesh of the ship from top

In Figure 22, mesh is finer closer to the hull; this is due to near-wall modeling to catch the viscous effects closer to hull. In addition, it is finer right after the hull, to catch wake and stern flow better in general. Unstructured grid is used in this case. In the Figure 23, mesh of the aft of the hull and actuators disks is seen.

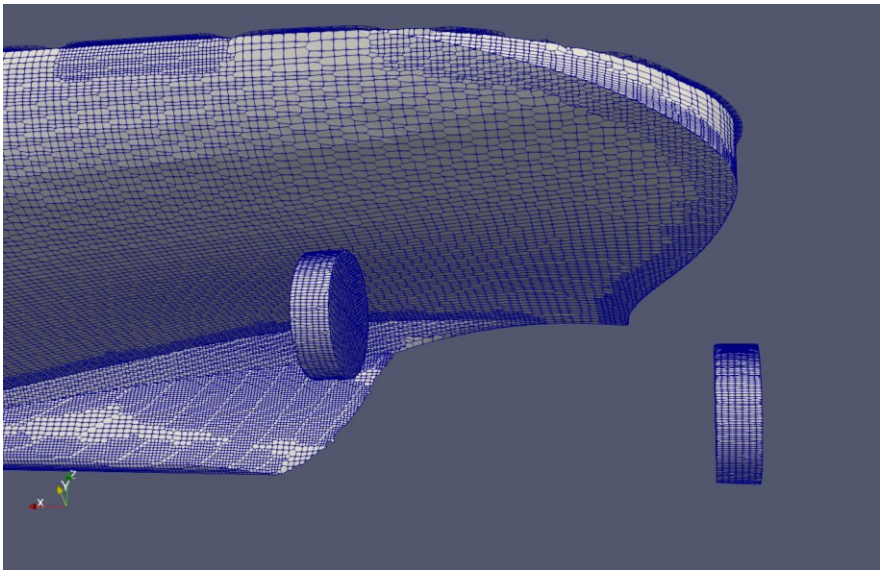

Figure 23 Mesh of the aft part of the ship and actuator disks

2.5.9 Discretization Scheme

Finite Volume Method (FVM) is used as discretization method. Other methods are Finite Element Method, Finite Difference Method, Spectral Element Method, Boundary Element Method and High-resolution discretization schemes. FVM is widely used in CFD with ships, since it has advantage with high Reynolds number turbulent flows, in memory usage and solution speed, especially for large problems compared to other methods.

In FVM method, the governing partial differential equations are recast in a conservative form and then solved over discrete control volumes. This guarantees the conservation through a control volume. Different discretization methods are used for different fields such as for free surface, continuity equation and common property of these is TVD that is used to solve these.

Discretization schemes for this thesis can be seen in the Appendix 3.

2.5.10 Fluid-Body Interaction

Hull has six degree of freedoms. In practice, it means that hull have surge, heave and pitch. Ship is symmetrical, there is no maneuvering or waves from external sources, so there is no yaw, roll, surge or sway motions. However, pitch and heave motions are taken into account in simulation.

3 Results

3.1 Actuator Disk Benchmark

Actuator disk was benchmarked against theoretical open water results of the propeller. The interest is how amount of cells in advance direction affects to the results. Table 5 indicates that finer grid to advance direction leads to more accurate results.

Table 5 Raw values of the actuator disk benchmark

	Cell amount Y-dir	r	J	T	Q	K_T	$10K_Q$	η_0
CFD	4	0.156	1.0057	0.0271	0.0018	0.0827	0.1796	0.7371
CFD	8	0.156	1.0045	0.0274	0.0019	0.0834	0.1807	0.7379
CFD	12	0.156	1.0026	0.0277	0.0019	0.0845	0.1825	0.7391
CFD	16	0.156	1.0014	0.0280	0.0019	0.0852	0.1836	0.7399
Theoretical	-	0.156	1.0000	0.0282	0.0019	0.0860	0.1848	0.7410

8-cell actuator disks were used in this thesis since it is accurate enough according to benchmark. These results are different that study [20] indicates that induced velocity is fractionally underestimated as advanced velocity is higher than theoretical value. Results differ, since advanced velocity calculation point is calibrated in this study.

3.2 New Concept

Four different models are used in the model tests: Base model, Model A, Model B and Model C. The Base Model has a conventional V-shaped aft body with three Azipod units; Model A has a tunnel shaped aft body with three Azipod units. In addition, Model B has the tunnel shaped aft body with two side Azipod units and one large CL propeller with a V-bracket and a modified center skeg. These models are used to compare traditional propulsion arrangements to new concept of the large centerline propeller. In addition, Model C is used in the boosting test. Model C (Figure 24) has the tunnel shaped aft body and two side Azipod units and large center line propeller. More detailed features are shown in the Table 6.

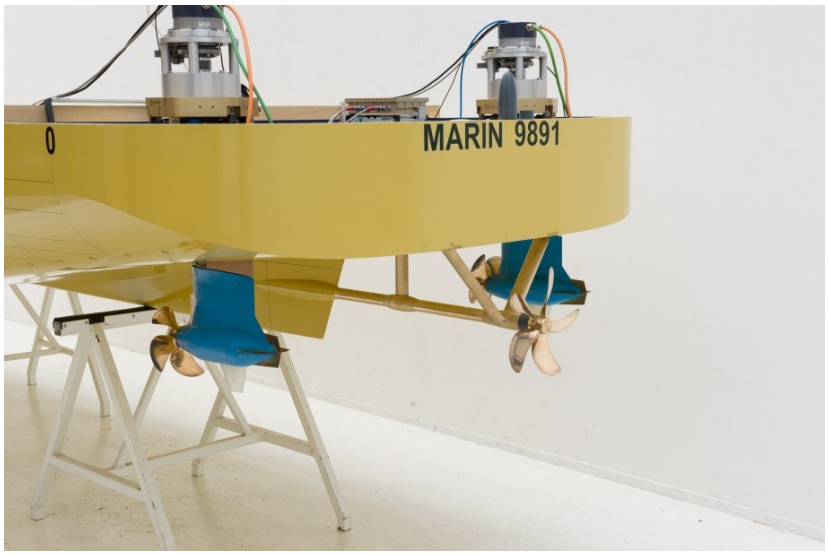

Figure 24 Aft configuration of the model

Table 6 Principal dimensions and arrangements of the used models

Model	Base Model	Model A	Model B	Model C	Unit
Length between perpendiculars	13.61	13.61	13.61	13.61	**m**
Lpp/B	7.253	7.253	7.253	7.253	**m**
B/T	5.333	5.333	5.333	5.333	**m**
Midship section coefficent	0.992	0.992	0.992	0.992	
Prismatic coefficent	0.703	0.703	0.703	0.703	
Waterplane coefficent	0.844	0.848	0.84	0.839	
Block Coefficent	0.697	0.697	0.698	0.698	**m**
Displacement	3052.46	3052.74	3054.25	3053.21	**m^3**
Wetted surface area	28.00	27.90	28.17	28.31	**m^2**
LCB position aft of FP	7.59	7.58	7.58	7.58	**m**
Aft shape	Conventional aft body	Tunnel shaped aft body	Tunnel shaped aft body	Tunnel shaped aft body	
Propulsion arrangement	3x POD Units	3x POD Units	2x POD Units & CL Propeller	2x POD Units & CL Propeller	
Side diameter	0.235	0.235	0.235	0.235	**m**
Mid diameter	0.235	0.259	0.311	0.313	**m**
Aft configuration	3x Azipod Headboxes I	3x Azipod Headboxes II	2x Azipod Headboxes II	2x Azipod Headboxes II	
			1 Shaft Arrangement I	1 Shaft Arrangement II	
				1 Ducktail I	
				1 Skeg II	

According to the model tests, there is a great difference in total shaft power when new centerline propulsion concept is introduced (Table 7 & Figure 25). The difference is the largest with the highest speed behalf of centerline propeller. In addition, tunnel shaped aft body improves the efficiency as Model A is better at almost every speed compared to base model. Figure 25 indicates that difference is not constant between the models. It is due to different aft configurations and propellers as their optimum velocities vary. In addition, larger mid propeller works better with higher speed since both Model B and Model C with larger mid propeller have relatively better efficiency with higher speed compared to models without large centerline propeller.

Table 7 Shaft power comparison versus base model in percentages according to model test results

Velocity (kn)	Model A	Model B	Model C
10	-1.14 %	-6.20 %	-7.02 %
12	-0.36 %	-7.11 %	-6.73 %
14	0.16 %	-6.87 %	-6.26 %
16	-0.48 %	-6.81 %	-5.65 %
18	-1.65 %	-7.43 %	-6.15 %
20	-1.54 %	-7.69 %	-6.87 %
22	-0.68 %	-7.72 %	-7.17 %
24	-0.35 %	-8.50 %	-8.02 %

Model B is slightly better than Model C, which has designed centerline propeller instead of stock propeller, however difference is due to different appendage configuration of Model B and Model C as Model C has a ducktail and different kind of skeg.

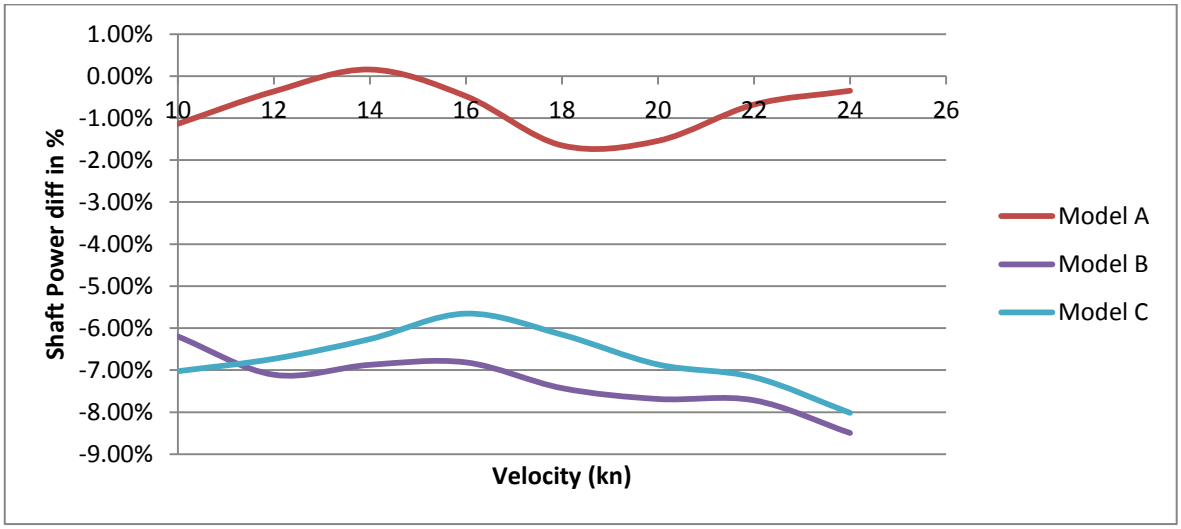

Figure 25 Shaft power comparison versus base model

Wake of centerline units for different models were compared to check if the position of the centerline propeller has an effect on wake. Wake fraction is significantly lower for Model B compared to base Model and Model A (Table 8). Tunnel shaped aft body improves wake as tunnel shaped aft body forms a low pressure that accelerates the flow. In addition, thrust deduction factor is more favorable with large centerline propeller as there are no clearance issues as discussed with [13].

MARIN itself has qualified resistance and propulsion test results as very good, that is the highest possible rating on their standards. Qualification bases on their statistical records for similar vessels as shown in [32].

Table 8 Wake comparison between models according to model tests

	Base Model	Model A	Model B
Velocity (kn)	Wake	Wake	Wake
10	0.13	0.091	0.042
12	0.125	0.089	0.044
14	0.12	0.087	0.045
16	0.115	0.085	0.047
18	0.111	0.084	0.048
20	0.107	0.082	0.05
22	0.103	0.081	0.051
24	0.1	0.08	0.053

3.3 Resistance

Table 9 presents raw data of the resistance results and comparison of the resistance results are shown in the Table 10. Results are compared in the model scale. Total resistance is approximately ten percentages lower than in the model tests, since CFD is done without appendages. CFD resistance is corrected with appendage effects in corrected resistance.

Appendage resistance for this type of cruise ships is ten to twenty percentages of the bare hull resistance as explained in [1]. Resistance is approximately nine percentages for the whole speed range for Base Model and Model A resistance in model tests. These models are lacking of a shaft arrangement, which is less energy efficient than pod housing as indicated in [1]. Appendage resistance was simulated to be 10.8 % for the whole speed range for Model C in CFD simulations. In addition, corrected resistance includes viscous scale effect on the resistance for both CFD and model tests. Viscous matches well with the model test results. It is unusual since appendages cause viscous resistance, however pressure resistance is significantly different. Corrected resistance is lower with higher speed compared to model tests, due reasons that corrected resistance is calibrated with speed of 18 knots and ratio of appendage resistance to total resistance is higher with lower speeds.

Table 9 Raw model test and CFD resistance values

Velocity (kn)	Resistance (N)	Viscous (N)	Pressure (N)	Corrected Resistance (N)	
18	67.9	63.1	4.8	49.3	**CFD**
18	75.2	63.0	12.2	49.3	**Model Tests**
22	98.5	91.4	7.1	71.9	**CFD**
22	110.4	91.6	18.8	73.2	**Model Tests**
20	81.9	76.5	5.5	59.4	**CFD**
20	91.7	76.7	15.0	60.3	**Model Tests**

Table 10 Resistance component comparison in percentages

Velocity (kn)	Resistance	Viscous	Pressure	Corrected Resistance
18	-9.73 %	0.19 %	-60.77 %	0.00 %
20	-10.65 %	-0.26 %	-63.24 %	-1.55 %
22	-10.78 %	-0.22 %	-62.23 %	-1.76 %

Resistance coefficients of CFD simulations and model tests for three different speeds are in the Table 11. Comparison in percentages is in the Table 12. The effective power is less than one percent with corrected resistance compared to the trials prediction of the model tests, which is rather good compared to study [17]. In addition, the different coefficients are rather close to each other, even if there are significant percentage differences for residual coefficient; however, the actual difference with residual coefficients is a lot lower than percentage difference indicates. Results follow the trend that higher velocity means higher underestimation in total resistance coefficient in model scale by CFD simulation as seen in studies [33] [34]. The difference is similar in total resistance coefficient model scale and full scale compared to studies [18] [34].

Table 11 Resistance coefficent comparison

Resistance	Velocity (kn)	C_{TM}	C_{FM}	C_R	C_{FS}	C_{TS}
CFD	18	317	267	20	144	209
Model	18	317	265	18	143	208
CFD	22	308	260	20	141	206
Model	22	312	258	21	140	207
CFD	20	310	263	17	142	205
MODEL	20	313	262	19	142	206

Table 12 Resistance coefficents difference comparison in percentages

Velocity (kn)	C_{TM}	C_{FM}	C_R	C_{FS}	C_{TS}	R_{TS} (kN)	P_E (kW)
18	0.06 %	0.85 %	9.74 %	0.54 %	0.72 %	0.77 %	0.79 %
22	-1.28 %	0.65 %	-4.48 %	0.43 %	-0.37 %	-0.28 %	-0.28 %
20	-1.04 %	0.47 %	-8.69 %	0.07 %	-0.38 %	-0.43 %	-0.41 %

3.4 Boosting

3.4.1 Model Tests

Boosting model tests results are provided in Appendix 3. The Table 13 and Figure 26 indicate that design power division is the most efficient till roughly 19 knots, when modified divisions of the power turn into more efficient solution. This concludes that boosting in operations could lead to fuel savings. When power is directed too much to the center propeller it is still less efficient than in the design power division.

Table 13 Shaft power comparison versus design power division in percentages

Power mid %	10 kn	14 kn	18 kn	22 kn
110	0.75 %	1.35 %	0.73 %	-1.53 %
130	0.78 %	1.27 %	0.55 %	-1.58 %
160	2.03 %	1.85 %	1.03 %	-0.87 %
200	4.39 %	4.09 %	3.89 %	1.61 %

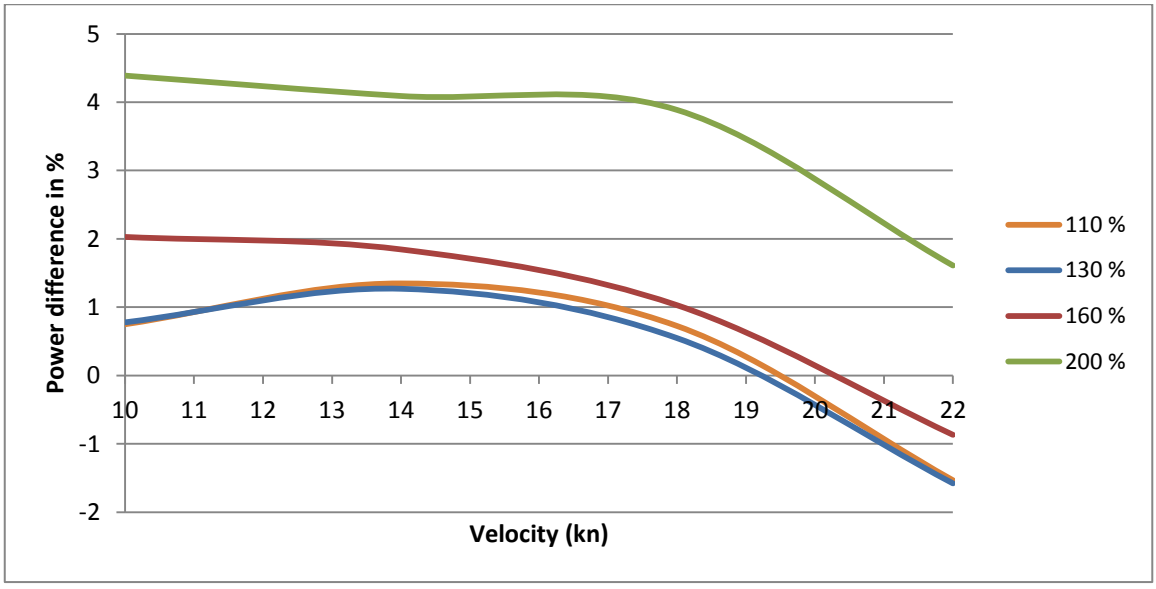

Figure 26 Boosting versus design power division according to model tests

3.4.2 CFD

In most cases thrust matches quite well with model test values since advance coefficient values are within one percent (Table 14). There is huge variation in wake and especially with thrust deduction, however it was anticipated that there will be problems with these coefficient. However, Table 15 indicates that actual difference with wake is rather small, except for design power division. Difference with setups between CFD simulation and model test is possible the reason behind the large difference rather than error in the model. Thrust deduction is rather inaccurate since corrected resistance is an educated guess. CFD is calibrated with model test values. It does not balance the resistance with thrust; therefore

thrust deduction is not trustworthy number in this case. To obtain thrust deduction, balancing the thrust and resistance in the simulation and most likely correct appendages are required. These results can be seen reasonable as difference between model test and CFD are within reasonable limits according to study [18]. However, wake fraction coefficient needs carefulness as it varies significantly even if difference is in within reasonable limits.

Table 14 CFD values compared to model test values in percentages

	POD	CL		POD	CL	POD	CL	Pod	CL	
kn/%	T	T	T total	J	J	η_0	η_0	w	w	t
18	-1.63	1.36	-0.52	0.58	0.14	0.01	0.20	-5.20	-1.72	-5.41
110	-1.83	-2.18	-1.97	0.57	0.61	0.02	0.15	-6.39	-6.48	-19.10
130	-2.20	-1.56	-1.91	0.71	0.52	-0.14	0.11	-8.16	-5.75	-18.64
160	-0.16	-0.87	-0.65	0.05	0.44	0.00	0.19	-0.54	-4.88	-6.32
200	1.43	-1.61	-0.67	-0.34	0.72	0.39	0.43	2.33	-7.69	-6.52
20kt	-1.32	-0.26	-0.93	0.43	0.06	0.01	0.04	-4.79	-0.59	6.27
22kt	-0.11	0.37	0.07	-0.02	-0.15	-0.01	0.06	0.24	1.55	16.76
110	0.06	0.29	0.15	-0.05	-0.08	0.01	0.03	0.55	0.79	19.59
130	0.30	1.08	0.65	-0.20	-0.31	0.09	-0.02	2.24	3.24	24.31
160	1.71	1.09	1.37	-0.58	-0.44	0.20	-0.22	6.73	4.68	30.16
200	4.31	0.45	1.65	-0.99	-0.18	1.06	-0.15	11.83	1.88	31.57

Resistance decreases while power in the mid propeller increases and it has a special effect on pressure resistance (Table 15). It is possible that mid propeller boosts the flow under the hull that reduces the pressure and therefore the resistance; however, this data is not sufficient to make valid reasoning why it is decreasing. In addition, the setup is not realistic, since shaft arrangement and pod housings are missing from the aft. Propulsion has effect only to pressure resistance as viscous resistance is virtually constant.

Table 15 CFD Calculation data

	POD	CL	Resistance In Newtons			Pod	CL	
Power	η_0 %	η_0 %	Total	Viscous	Pressure	w	w	t
design 18kn	66.6	75.3	70.1	63.1	6.9	0.0758	0.0887	0.0839
110	66.6	75.3	69.9	63.1	6.8	0.0773	0.0799	0.0769
130	66.5	74.8	69.9	63.1	6.8	0.0740	0.0789	0.0770
160	65.9	73.6	69.9	63.2	6.7	0.0764	0.0785	0.0884
200	63.1	71.9	69.7	63.2	6.6	0.0757	0.0766	0.0877
design 20kn	66.6	75.3	85.2	76.8	8.4	0.0792	0.0893	0.0972
110	66.6	75.2	85	76.6	8.4	0.0803	0.0638	0.0964
130	66.5	74.6	85.1	76.8	8.3	0.0809	0.0895	0.0960
160	65.7	73.4	84.9	76.8	8.1	0.0797	0.0892	0.0950
200	62.6	71.6	84.6	76.8	7.8	0.0820	0.0892	0.0965
design 22kn	66.6	75.2	102.7	91.7	11.1	0.0852	0.0900	0.1150
110	66.6	75.2	102.7	91.7	11	0.0846	0.0898	0.1060
130	66.6	74.6	102.5	91.6	10.9	0.0841	0.0902	0.1115
160	66.0	73.3	102.2	91.5	10.7	0.0853	0.0900	0.1208
200	63.7	71.5	101.8	91.4	10.4	0.0867	0.0887	0.1262

Wake of the centerline propeller was compared to model tests as it influences on the propeller. Figure 27 shows that it matches well for boosting power division. There is a slight variation for design power division, however the most important aspect is that it lines well with boosting power divisions.

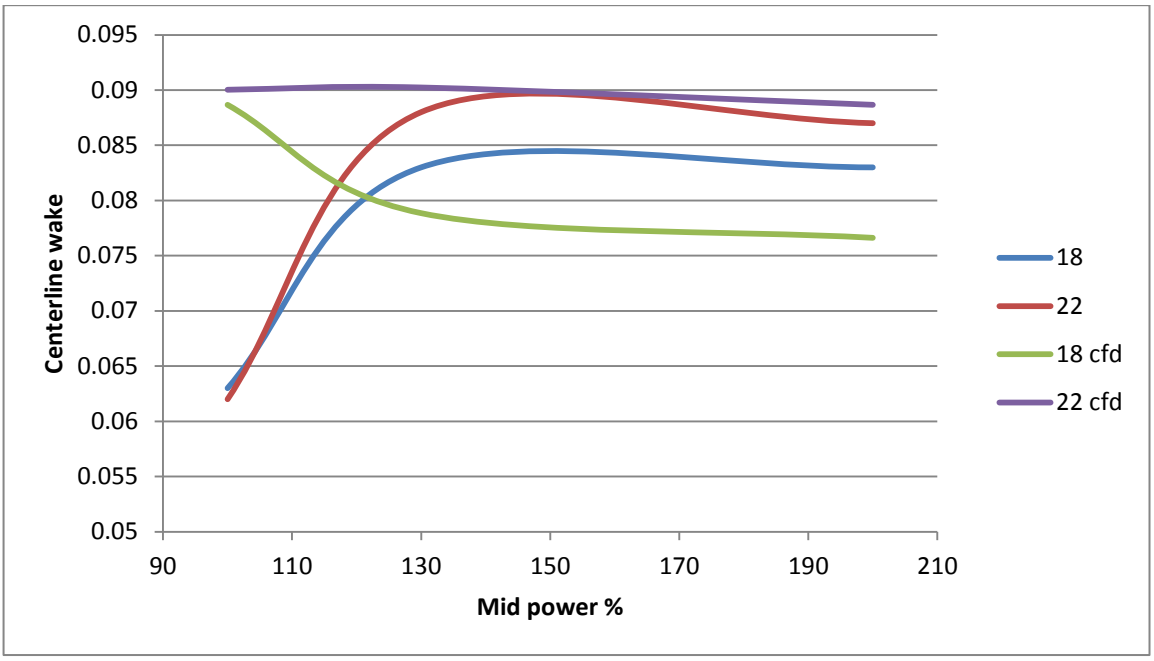

Figure 27 Wake comparison

Following tables (Table 16, Table 17 & Table 18) provides power distribution comparison between CFD calculations and model tests according to K_Q methods. Optimum power distribution according to Matlab simulation is compared with CFD in every case. Model test data does not contain boosting data for 20 knots; only design power division is compared to model test data in that case.

Simulation was calibrated with speed of 18 knots. Power distribution from CFD matches well with values from model tests. Difference is from one percentage point to three percentage points, however difference between side units and mid units are lower with CFD than in model test. Difference is rather constant. Interesting point is that Matlab optimum is matching with CFD simulations, even if Matlab simulation is rather rough.

Table 16 CFD Comparison to model test data according to K_Q -method for 18 knots

KQ Method	Power Distribution (CFD)		Power Distribution (Model tests)	
18 kn	**Side**	**Mid**	**Side**	**Mid**
Design	99 %	103 %	98 %	104 %
110	96 %	107 %	95 %	110 %
130	86 %	128 %	85 %	130 %
160	71 %	158 %	70 %	160 %
200	51 %	197 %	50 %	200 %
Matlab Opt.	79 %	143 %	79 %	143 %

Same applies for 22 knots as for 18 knots, difference between CFD and model tests are within one to two percentage points and CFD is underestimating power difference and Matlab optimum is still matching well.

Table 17 CFD Comparison to model test data according to K_Q -method for 22 knots

KQ Method	Power Distribution (CFD)		Power Distribution (Model tests)	
22 kn	**Side**	**Mid**	**Side**	**Mid**
Design	97 %	106 %	96 %	108 %
110	96 %	108 %	95 %	110 %
130	86 %	129 %	85 %	130 %
160	71 %	158 %	70 %	160 %
200	51 %	197 %	50 %	200 %
Matlab Opt.	78 %	143 %	79 %	142 %

Power distributions matches well (Table 18), even if simulation setup for 20 knots was calibrated with Matlab simulation code instead of model test results.

Design power division is not the same for every speed in the model tests as power in the mid propeller increases one percentage point per knot (Table 18). Design power division is not even since hull of the ship directs the flow better to the mid propeller and due to propeller interaction as concluded in [19].

Table 18 CFD Comparison to model test and Matlab data according to K_Q -method for 20 knots

KQ Method	Power Distribution (CFD)		Power Distribution (Model tests/matlab)	
20 kn	**Side**	**Mid**	**Side**	**Mid**
Design	98 %	104 %	97 %	106 %
110	91 %	118 %	95 %	110 %
130	84 %	132 %	85 %	130 %
160	69 %	162 %	70 %	160 %
200	49 %	201 %	50 %	200 %
Matlab opt.	78 %	144 %	79 %	142 %

Power division with simplified CFD simulation matches well with model test results according to tables Table 16, Table 17 and Table 18, therefore CFD model is accurate enough to model different power divisions.

Shaft powers, which are obtained with various different methods: K_Q -method with CFD, Matlab simulation and model tests, are compared. Table 19 provides information, where CFD and K_Q -method from model tests are compared. There is a large variation with 18 knots, even if power distribution was rather close to each other. In addition, CFD is under estimating shaft power compared to model tests.

For 22 knots difference is significantly lower than for 18 knots. CFD simulations tend to overestimate the power when power is increased. Same applies for the 18 knots. Advanced calculation point is the probable cause as it stays still when power distribution is changed. Mid unit is boosting the flow which leads to increasing the advanced velocity since calculation points keeps the position. For side unit advanced velocity decreases as propeller is

not boosting that much flow anymore. There are two side units and one center unit in the simulation, therefore the total power increases more than it should.

For 20 knots it is under estimating the shaft power and for this case there is no boosting comparison as there is no model tests for speed 20 for boosting.

Table 19 CFD Comparison to model test data according to K_Q -method

CFD vs KQ Method	Total Shaft Power Difference to Model Tests		
Velocity (kn)	**18**	**22**	**20**
Design Power Division	-4.3 %	-0.9 %	-1.6 %
110	-2.1 %	-0.2 %	-
130	-2.3 %	0.2 %	-
160	-1.0 %	0.8 %	-
200	-1.1 %	0.8 %	-

There is an error calculation (Figure 30) for design power division for 18 knots as it differs significantly. Table 20 and Table 18 support this theory as CFD comparison to Matlab simulation data significantly differ from compared to other speeds and power divisions. This specific situation was simulated twice with CFD and Matlab. This indicates that problem is in CFD setup or in CFD simulation itself, however as other values matches well with each other and other simulations the error is most likely in input values of the CFD that are put by user.

Estimates from Matlab simulation are close to CFD values (Table 20). Differences are mostly less than one percentage point. There is variation if CFD is over or under estimating the shaft power compared to Matlab simulation. It indicates that there is more room for error in Matlab simulation as the model test data are most likely more accurate and there was a clear trend where CFD and model tests were compared.

If design power division for 18 knots is excluded the difference is from -2.3% percentage point to 0.8 percentage point. According to study [17], this can be qualified as sufficiently high accuracy for self-propulsion and definitely accurate enough to study boosting.

Table 20 CFD Comparison to Matlab simulation

CFD vs Matlab	Total Shaft Power Difference to Matlab simulation		
Velocity (kn)	**18**	**22**	**20**
Design Power Division	-3.78 %	-0.34 %	-0.97 %
110	-0.96 %	-1.32 %	2.02 %
130	-0.71 %	-0.68 %	-1.25 %
160	0.51 %	0.41 %	-1.09 %
200	0.80 %	1.26 %	-0.68 %
Matlab optimum	-2.87 %	-0.66 %	-1.30 %

Boosting curves of different methods were compared with model tests (Figure 28), CFD (Figure 29) and CFD (Figure 30) with added 20 knots Matlab calibrated point.

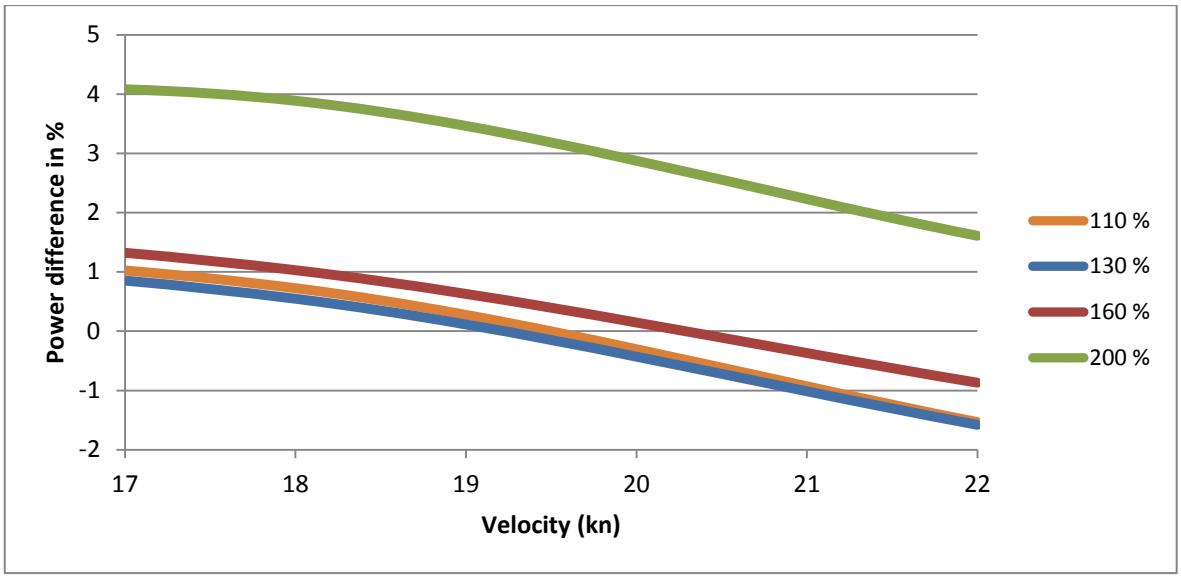

Figure 28 Boosting versus design power division in model tests

Trend of boosting curves are equivalent for CFD and model tests, even if there is slight variation with differences. Model test shows that 130% is the most efficient, even if the difference with the 110% is really small, however CFD shows that 110% is the most efficient, even if 130% is close in this case. However the difference is so small that no final conclusions can be made which one is better in the end.

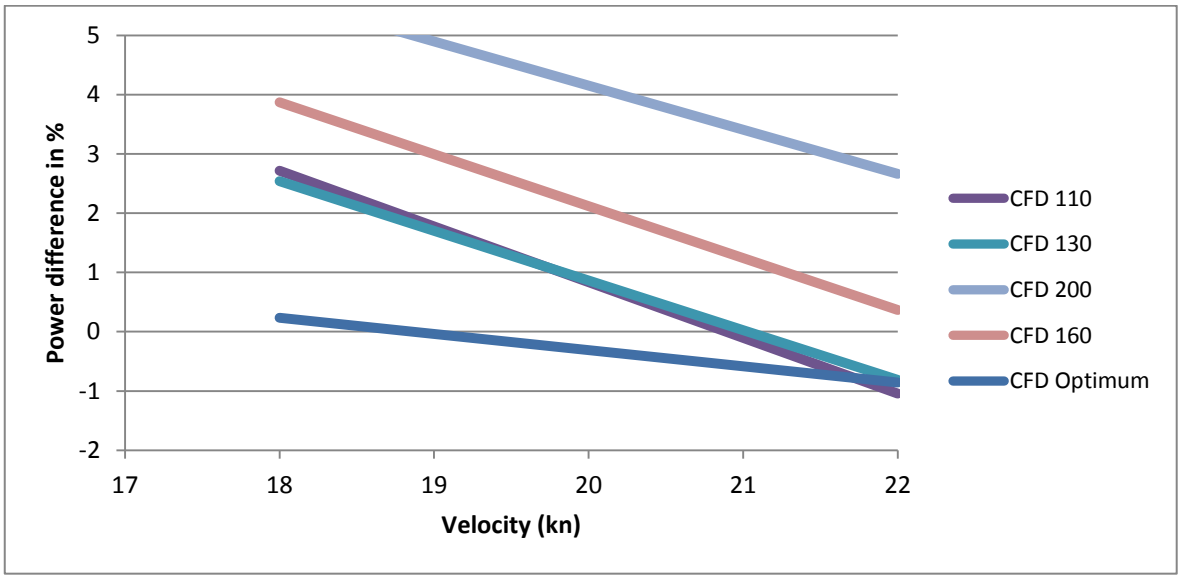

Figure 29 Boosting versus design power division in CFD tests

Additionally, Figure 30 contains the Matlab calibrated 20 knots points. There is no model test data for this; however it was checked how well it matches with interpolated model test curves. In this case CFD 110 % point for 20 knots is invalid due to unknown error. When Matlab simulation code is used for calibrating, it under estimates the difference as every curve is decreasing more than it should according to trend. It does not have an effect on the trend of which boosting condition is the most favorable. When these points are compared to interpolated model test values (Table 21), these values matches quite well. The trend is the same.

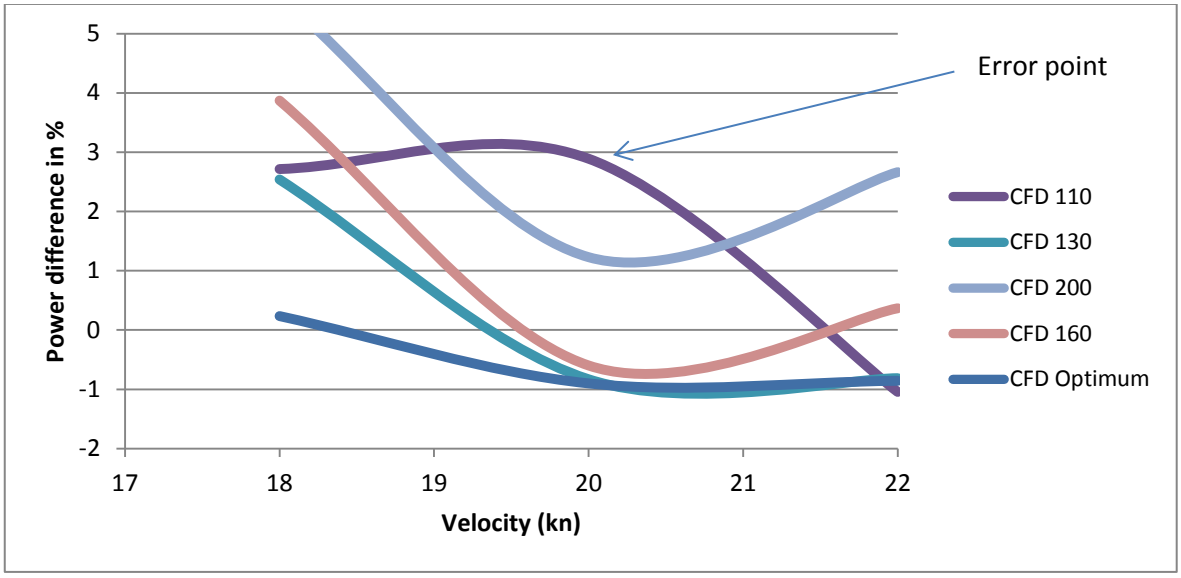

Figure 30 Boosting versus design power division in CFD tests with 20 knots Matlab calibrated point

Table 21 Total Shaft Power for 20 knots

Mid power (%)	Interpolated Model tests (%)	CFD (%)
110	-0.4	2.9
130	-0.5	-0.8
160	0.1	-0.6
200	2.6	1.2

3.4.3 Matlab Simulation

Results are rather close to each other (Table 22). Maximum difference between Matlab simulation and model tests is an only 1.9 percentage point that is rather low difference as Matlab simulation is the most time efficient solution.

Table 22 Matlab simulation versus model tests according to K_Q -method

Matlab vs KQ Method	Total Shaft Power Difference to Model Tests		
Velocity (kn)	**18**	**22**	**20**
Design Power Division	-0.6 %	-0.6 %	-0.6 %
110	-1.2 %	1.2 %	-
130	-1.6 %	0.9 %	-
160	-1.5 %	0.4 %	-
200	-1.9 %	-0.4 %	-

The largest difference with Matlab simulation compared to model test and CFD are the power distribution curves. Overall trend is the same (Figure 31), when it is compared what power distribution is the most efficient. Matlab simulation is indicating that higher speed means that difference gets lower. The differences with the power are lower as for worst case (200%) difference to design power division is only one percentage point and the most efficient is close to 0.5 % percentage point. In addition, power curves are rather straight lines without steps as in model tests and CFD. However, when total shaft power difference to model tests is compared (Table 22), the difference fluctuates from -1.9 percentage points to 0.9 percentage points. This has better accuracy than with CFD simulation.

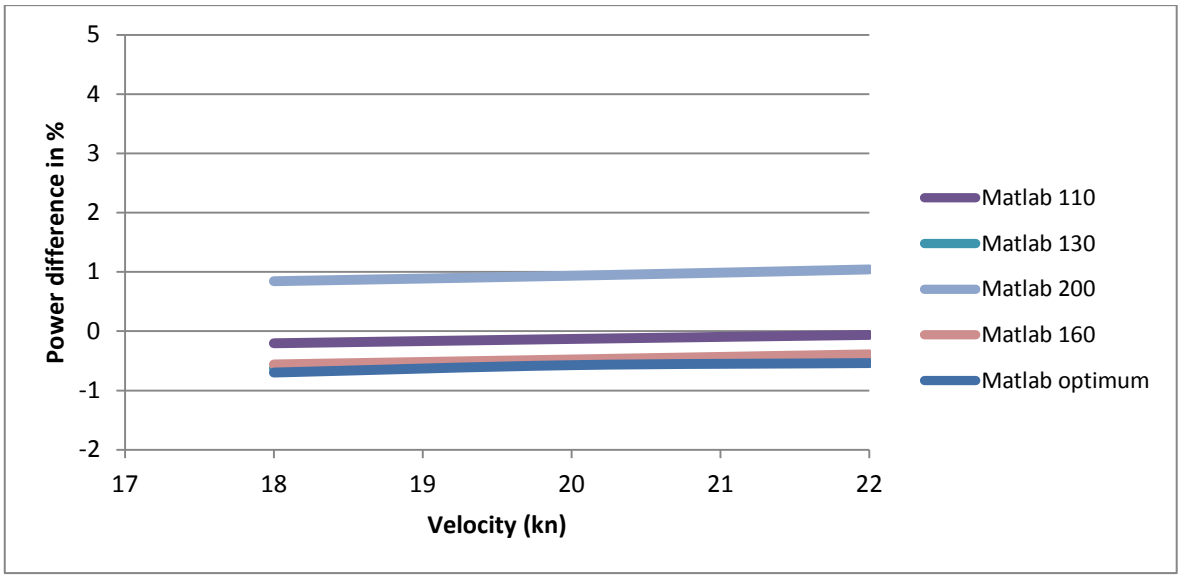

Figure 31 Boosting versus design power division with Matlab simulation

3.4.4 Calculation Times

CFD simulation takes approximately 4 hours to stabilize that results are reliable. It takes approximately 1 hour and thirty minutes to stabilize if simulation is already calibrated and only RPM is changed. In practice, to model one speed and one power division from scratch, it takes approximately eight hours to do simulations, as one base run and one calibrating RPM run are needed, so final values can be interpolated. In addition, it needs one run to check that it is calibrated correctly. However, one Matlab simulation takes only less than one minute, which is significantly lower than CFD simulation (Table 23).

Table 23 Approximate simulation times with CFD and Matlab simulation

Explanation	Time
CFD from point zero	4h 10min
CFD One boosting run	1h 37min
Matlab simulation	< 1 min

4 Discussion

4.1 Simulation Models

There is a variation with the shaft power estimations; nevertheless the trend of the different boosting conditions is equal in model tests, Matlab simulations and CFD simulations. However, this study consists of only one hull. Results should be verificated by testing with other models and individual simulating of CFD and Matlab simulation without prior data from model tests. In addition, the most efficient procedure to do simulations is by increasing the complexity of the simulation setup while decreasing the amount of possible choices of the design power divisions.

It is sufficient to first model the boosting trends with Matlab simulation code and then utilize CFD simulation to verify the most interesting boosting cases in the scope of this thesis. In the later stage these CFD results can be verified with model tests and full scale tests. Same optimization strategy is used in automated hull optimization, where simpler tool such as potential flow CFD code is used to restrict the design space. In the following step the most efficient hull form options are verified with more advanced tool such as RANS based CFD code as discussed in [35].

Propulsion has an effect only on the pressure resistance. It is most likely since propulsion units are affecting on the streamlines, which increases pressure resistance. In addition, higher load in the mid unit lowers the pressure resistance. There could be two reasons explaining this phenomena. One reason is that shaft arrangement is missing and other one is the mid propeller boosts the effect of the tunnel stern that lowers the pressure in the aft.

4.2 Boosting

Boosting is an efficient option with higher speeds according to this study with limited amount of results. Results indicate that the optimum power division changes with speed, therefore boosting is most likely more efficient in operations than in ship design in early phase. Modifying of the propulsion units loads can lead to the savings during operation when speed varies. However, propellers can be designed for boosting condition, and then speed can be rather constant.

These simulations indicate only one percentage point power difference at maximum for 22 knots. For a large cruise ship it can lead to high amount of savings per year. There could be even more gain for fast ferries due to higher speeds. In addition, these propellers in these tests were not designed for boosting situation. Appropriate propeller design could lead to even one to three percentages efficiency as discussed with Meyer Turku Head of Hydrodynamics [13], however this should be tested with CFD and model tests.

Open water curve has large influence on the effect of boosting as the flatter top on the open water curve means that there is more room to modify the loading of the propeller, therefore propellers should be designed from the perspective of boosting.

Boosting could be especially meaningful for the crafts that have varying operational profile such as multipurpose vessels that break ice during the winter and offshore missions during the summer, and then different propulsion loads could be effective in efficient operations, even if the propellers are not designed for boosting.

4.3 Ship

Estimating the actual fuel consumption per year is complex subject since it is dependent on the operational profile of the vessel that can vary significantly; however conservative estimation of the savings per year was done to give rough example. Harmony of the Seas was taken as a case to estimate savings during the year as a rough example. Harmony of the Seas is one of the largest cruise ships in the world with 226 963 GT. Total propulsion power of the Harmony of the Seas is 60 MW (100% MCR). Ship has six engines: four times Wärtsilä 12V46F and two times Wärtsilä 16V46F. These engines have same SFOC that is 170g/kWh according to specifications of the engine [36]. It is assumed that ship uses approximately 60% of the total propulsion power four hours per day in a year. She consumes 8935 tons per year of MGO/HFO. Price of the HFO is $470 per ton as shown in the [37], it leads to $4200000 fuel consumption per year. Model tests shows that shaft power is more than four percentages less for every speed for tunnel stern with centerline propulsion compared to V-stern. This already leads to $210000 fuel cost savings per year. When boosting for 20 or 22 knots is taken into account saving per year can be $42000 higher as power difference is approximately one percentage point higher, however this assumption includes that ship sails with at least 20 knots four hours per day. This is a rough estimate and includes conservative fuel HFO that is the most environmentally consuming fuel and the cheapest.

One downside with centerline propeller is that it is heavier solution than with three pod units due to large shaft that is needed with centerline propeller; nevertheless centerline propeller is more efficient according to the results.

4.4 Problems

Propulsion factors are calculated with one point, which means that calibrating upper velocity point is important. Calibrating of the point is challenging, since propeller is affecting on the stream and if point is too far from the propeller wake effect is lost. One solution is to handle the points as a disk, where average is taken and it is used as an upper velocity point. It could lead to setup the point easier. Other way is to make simulations with multiple different hulls and try to find semi-empirical formula how to find the correct points with a formula. Second problem is that actuator disk does not act in the heterogeneous wake. In real case K_T and K_Q changes compared to open water results due to the wake, since flow is not uniform. Actuator disk does not take this into account; therefore there is error in the thrust values.

There are some uncertainties, since some effects are missing in the simulations due to bare hull simulation. The largest reason is that shaft arrangement in front of mid propeller is missing.

4.5 Error Sources

4.5.1 Model Tests

Model tests are kept rather accurate way to predict performance of the vessel; however they are still problematic as there are scaling issues (2.4). In addition, it is experience based estimation. There is larger uncertainty with new concepts due to experience factor of scaling as discussed in [28]. To avoid errors CFD should be compared to full scale results that are not available with new concepts. In theory, it could be that CFD results are closer to

full scale results than model scale results are. However, current trend is that model tests are considered more accurate and they are easy way to validate CFD in this case, as model tests are done by the experienced model basin, so accuracy is sufficient for this preliminary study. Full scale experiments have their own difficulties as it is practically impossible to find unrestricted sea area, where are no waves or wind to get real values for calm water, however it is seen that it can be done reliable.

4.5.2 CFD

The major error sources are due to that model is really simplified; therefore results should be validated with better CFD model or with model tests. One problem with comparison is that situation is different with model test and CFD. Model test situation has appendages and CFD is without. The largest problem is that RPM of the propellers are defined with values from model tests. It means that thrust is not matching the resistance that is result of CFD simulations. It is tried to compensate with the factor of corrected resistance that is used to calculated thrust deduction factor but at best it is just a well-educated guess. One other option could have been to compare CFD resistance with resistance values from the self-propulsion situation, as then it is seen how much propulsion adds resistance, however it was more far from the model test results than this well-educated guess. It would be important to balance the resistance with thrust in CFD simulation.

5 Future Work

CFD and Matlab simulation code should be tested without relying on the model test data and later compare obtained results to model test or full scale test data. These models should be tested with different type of hulls and larger speed range to validate model and to check if boosting is relevant only with higher speeds as with this model in this thesis. In addition, effects of pod direction should be studied, how this affect to load change. Matlab optimum should be verificated with model tests. In addition, different types of propellers should be tested to check which one gives the best performance for boosting in the designed condition.

Several of different hulls should be tested to obtain semi-empirical formula for the advanced velocity calculation point to minimize the error in the simulations. In addition, shaft arrangement in front of propulsion should be added to the simulation as it has a large effect on streamlines.

One interesting research topic is to study faster ferries such as Tallink Megastar with CFD and modify it to use two smaller pods and large centerline propeller in order to have better comparison with current state-of-the-art solutions.

References

[1] R. Hämäläinen and J. van Heerd, "Energy saving possibilities in twin or triple propeller cruise liners," in *Third International Symposium on Marine Propulsors*, Launceston, 2013.

[2] U. Hollenbach and O. Reinholz, "Hydrodynamic Trends in Optimizing Propulsion," Second International Symposium on Marine Propulsors, Hamburg, 2011.

[3] IMO, "Prevention of Air Polluttion from Ships," IMO, 2018.

[4] Z. Bazari and T. Longva, "Assesment of IMO Mandated Energy Efficiency Measures for International Shipping," DNV-GL, 2011.

[5] 2H Offshore, "2H Offshore," [Online]. Available: https://2hoffshore.com/services/production-export/riser-concept-engineering/concept-eng-cost-influence-curve/. [Accessed 17 August 2018].

[6] USCGA, "Small Craft Facility Training Guide," United States Coast Guard, 2009.

[7] A. Molland, T. S and D. Hudson, "Hull Form Design," in *Ship Resistance and Propulsion*, Cambridge University Press, 2017, pp. 332-358.

[8] J. Rogers, "The Different Types of Yacht Propulsion: Benefits and Drawbacks".

[9] Super Yachts, "Super Yachts," 24 July 2018. [Online]. Available: http://www.superyachts.com/motor-yacht-2619/ecstasea.htm.

[10] Wärtsilä, "Wärtsilä Encyclopedia of Marine Technology, Coastguard vessel K/V Turva," Wärtsilä, [Online]. Available: https://www.wartsila.com/encyclopedia/term/coastguard-vessel-k-v-turva. [Accessed 28 August 2018].

[11] Baltic Yachts, "Baltic Yachts Unveil Revolutionary Retractable Propulsion System," 24 July 2018. [Online]. Available: https://www.balticyachts.fi/baltic-yachts-unveil-revolutionary-rectractable-propulsion-system/.

[12] MARIN, "Performance tests with four propulsion concepts and aftbody designs," MARIN, Wageningen, 2018.

[13] R. Hämäläinen, Interviewee, *Head of Hydrodynamics, Meyer Turku.* [Interview]. 29 August 2018.

[14] A. Techer, *2.016 Hydrodynamics,* 2005.

[15] J. Matusiak, Short Introduction to Ship Resistance and Propulsion, 2008.

[16] W. e. al, "Free Surface Viscous Flow Solution Methods for Ship Hydrodynamics," *Archives of computational Methods in Engineering,* vol. 18, no. 1, pp. 1-41, 2011.

[17] V. Krasilnikov, "Self-Propulsion RANS Computations with a Single-Screw Container Ship," Third International Symposium on Marine Propulsors, Launceston, 2013.

[18] J. Choi, H. Lee, J. Kim, Lee and D, "Computational predictions of ship-speed performance," *Journal of Marine Science and Technology,* vol. 14, no. 3, pp. 322-333, 2009.

[19] Z. Z, Z. Hong, H. Zhang and P. Sahoo, "An investigation of load change of propeller in four-propulsion vessel using CFD," *Journal of Marine Science and Technology,* vol. 23, no. 1, pp. 122-131, 2008.

[20] Q. Gao, W. Jin and D. Vassalos, "The calculations of propeller induced velocity by RANS and momentum theory," *Journal of Marine Science and Application,* vol. 11,

no. 2, pp. 164-168, 2012.

[21] MAN Diesel & Turbo, "Basic Principles of Ship Propulsion," MAN.

[22] MathWorks, "MathWorks Documentation," 20 July 2018. [Online]. Available: https://se.mathworks.com/help/optim/ug/fmincon.html.

[23] V. Bertram, Practical Ship Hydrodynamics, Oxford: Butterworth-Heinemann, 1999.

[24] A. Sandqvist, *Sea Trial Academy, Hydrodynamic lecture,* Turku: Meyer Turku, 2018.

[25] Centrale Nantes, "Theoretical Manual, ISIS-CFD v6.2," 2017.

[26] V. L. Lazauskas, "Resistance, Wave-Making and wave-Decay of Thin Ships, with Emphasis on the Effects of Viscosity," The University of Adelaide, Adelaide, 2009.

[27] ITTC, "Resistance Uncertainty Analysis, Example for Resistance Test," ITTC, 2002.

[28] H. Raven, A. van der Ploeg, A. Starke and L. Eca, "Towards a CFD-Based Prediction of Ship Performance --- Progress in Predicting Full-Scale Resistance and Scale Effects," Marin, Wageningen, 2008.

[29] L. Larsson and H. C. Raven, "Numerical Prediction of Resistance and Flow Around the Hull," in *Principles of Naval Architecture Series: Ship Resistance and Flow*, Jersey City, The Society of Naval Architects and Marine Engineers, 2010, pp. 107-155.

[30] H. Jun-Ming, L. Tie-li, L. Yan, G. Guan and Z. Zi-bo, "Prediction of ship power and speed performance based on RANS method," *International Shipbuilding Progress,* vol. 64, no. 1-2, pp. 51-78, 2017.

[31] T.-Y. Lin and J.-S. Kouh, "On the scale effect of thrust deduction in a judicious self-propulsion procedure for a moderate-speed containership," *Journal of Marine Science and Technology,* vol. 20, no. 2, pp. 373-391, 2015.

[32] Marin, "Large Design Centre Proepller Performance, Cavitation and Noise Measurements, Final Report," Marin, Wageningen, 2018.

[33] D. Ponkatrov and C. Zegos, "Validation of Ship Scale CFD Self-Propulsion Simulation by the Direct Comparison with Sea Trials Results," Fourth International Symposium on Marine Propulsors, Austin, 2015.

[34] X. Shi, X. Chen and J. Tan, "Study of resistance performance of vessels with notches by experimental and computational fluid dynamics calculation methods," *Journal of Shanghai Jiatong University,* vol. 15, no. 3, pp. 340-345, 2010.

[35] J. Maisonneuve, S. Harries, J. Marzi, H. Raven, U. Viviani and H. Piippo, "Towards Optimal Design of Ship Hull Shapes," International Marine Design Conference, Athends, 2003.

[36] Wärtsilä, "Wärtsilä 46F Product Guide," Wärtsilä, Marine Solutions, Vaasa, 2017.

[37] Ship and Bunker, "World Bunker Prices," Ship and Bunker, [Online]. Available: https://shipandbunker.com/prices. [Accessed 1 August 2018].

[38] ITTC, "Testing and Extrapolation Methods, Propulsion, Performance Propulsion Test," ITTC, 2008.

Appendix

Appendix 1. Matlab Simulation Script, 6 pages
Appendix 2. Discretization Schemes, 1 page
Appendix 3. Boosting Results (Model Tests), 2 page

Appendix 1. Matlab Simulation Script

Main file

```
format long
format compact
clear all

global PS1 PS2

Cf=-0.74*1000;              % Adjust that in default condition re-
sistance difference is 0 , -1.83 (20kt), -.74(18), -0.68(22kt)
PE=15674*1000;              % Effective Power
Vs=18;                      % Ship speed in knots
THDF=0.085;                 % Thrust deduction factor, 0.085 as de-
fault
d1=8;                       % Diameter MID in m
d2=6;                       % Diameter POD in m
FD=0;                       % Frictional scaling factor (Model scale
only), XXX percentage of total as default, kokeile kayttaa scaling
factoria
lambda=25.573;              % Scaling factor
roo=1025.9;                 % Density in kg/m^3

knottoms=0.51444444;        % Translation from kt to m/s
r=PE/(Vs*knottoms);         % Resistance

Va1=(0.0929*Vs-0.0049)*sqrt(lambda);    % Advanced velocity in m/s for
MID
Va2=(0.0916*Vs+0.0303)*sqrt(lambda);    % Advanced velocity in m/s for
POD

rm=(r-FD)/(1-THDF)+Cf;      % Required thrust

xo=[0.925; 0.923];                      % Guess balues for J
xmin = [0;0];                           % Min allowed value for J:s
xmax = [2;2];                           % Max allowed values for J:s

% Set some optimisations options to show intermediate results

options = optimset;
options.Diagnostics = 'on';
options.Display = 'iter';
options.MaxFunEvals = 2000;
options.TolFun = 1e-20;
options.TolCon = 2;
options.TolX = 1e-200;

[x,fval,exitflag, output, lambda] = fmincon('obf', xo, [], [], [],
[], ...
  xmin, xmax, 'nonlcon', options, d1, d2, Va1, Va2, rm,roo);


% Write some results to screen

---CUT---
```

Objective function file

```
function PStot = obf(x,d1, d2, Va1, Va2, rm, roo)
  % Objective function for optex, Minimizing the total power
global PS1 PS2

J1=x(1);
J2=x(2);

n1=Va1/(d1*J1);
n2=Va2/(d2*J2);

% Propeller curves

KT1=0.0184*J1^6+0.0959*J1^5-0.5362*J1^4+0.7778*J1^3-0.5816*J1^2-
0.1752*J1+0.4868;
KQ1=0.0022*J1^6+0.0292*J1^5-0.1126*J1^4+0.1228*J1^3-0.0682*J1^2-
0.029*J1+0.074;
KT2=-0.0093*J2^6+0.1719*J2^5-0.6038*J2^4+0.7315*J2^3-0.3705*J2^2-
0.3672*J2+0.5924;
KQ2=0.0453*J2^6-0.0171*J2^5-0.3249*J2^4+0.5746*J2^3-
0.3571*J2^2+0.0261*J2+0.0887;

% KQ-method calculation for Shaft power

PS1=KQ1*n1^3*d1^5*roo*2*pi()/0.99;
PS2=2*KQ2*n2^3*d2^5*roo*2*pi()/0.995;

PStot=PS1+PS2;
```

Thrust and power calculation file

```
function g = propeller(x,props)

d1=props(1);
d2=props(2);
Va1=props(3);
Va2=props(4);
rm=props(5);
roo=props(6);

J1=x(1);
J2=x(2);

n1=Va1/(d1*J1);
n2=Va2/(d2*J2);

% Propeller curves

KT1=0.0184*J1^6+0.0959*J1^5-0.5362*J1^4+0.7778*J1^3-0.5816*J1^2-
0.1752*J1+0.4868;
KQ1=0.0022*J1^6+0.0292*J1^5-0.1126*J1^4+0.1228*J1^3-0.0682*J1^2-
0.029*J1+0.074;
KT2=-0.0093*J2^6+0.1719*J2^5-0.6038*J2^4+0.7315*J2^3-0.3705*J2^2-
0.3672*J2+0.5924;
KQ2=0.0453*J2^6-0.0171*J2^5-0.3249*J2^4+0.5746*J2^3-
0.3571*J2^2+0.0261*J2+0.0887;

% KQ-method calculation for Shaft power
```

```
PSMID=KQ1*n1^3*d1^5*roo*2*pi()/0.99;  % CL Shaft efficiency 99%
PSPOD=2*KQ2*n2^3*d2^5*roo*2*pi()/0.995; % Pod Shaft Efficiency 99.5%

T1=KT1*roo*d1^4*n1^2;     % Thrust in N MID
T2=KT2*roo*d2^4*n2^2;    % Thrust in N Side
Ttotal=T1+T2*2;         % Total Thrust of the ship

g=[Ttotal, PSMID, PSPOD];

end
```

Constraint function file

```
function [c,ceq] = nonlcon(x,d1, d2, Va1, Va2, rm,roo)

props=[d1 d2 Va1 Va2 rm roo];
g = propeller(x,props); % Constraints

PSTOT=g(2)+g(3);
PSDIVMID=g(2)/PSTOT*3;
PSDIVSIDE=g(3)/PSTOT/2*3;

c(1)=-g(1)+rm;   % To balance thrust with resistance

% When certain power division is desired

%c(2)=PSDIVMID-2;
%c(3)=PSDIVSIDE-0.5;

% When optimum power division is desired

c(2)=-PSDIVMID;
c(3)=-PSDIVSIDE;

ceq = [];
end
```

Example of the output of the program

```
_____________________________________________________________________
_
   Diagnostic Information

Number of variables: 2

Functions
Objective:                                  obf
Gradient:                                   finite-differencing
Hessian:                                    finite-differencing
(or Quasi-Newton)
Nonlinear constraints:                      nonlcon
Nonlinear constraints gradient:             finite-differencing

Constraints
Number of nonlinear inequality constraints: 3
Number of nonlinear equality constraints:   0
```

```
Number of linear inequality constraints:    0
Number of linear equality constraints:      0
Number of lower bound constraints:          2
Number of upper bound constraints:          2

Algorithm selected
   interior-point


_____________________________________________________________________
_
   End diagnostic information
                                                        First-order
Norm of
 Iter F-count            f(x)  Feasibility   optimality
step
    0       3    2.274443e+07    6.856e+03    2.949e+06
    1      15    2.280313e+07    0.000e+00    2.588e+06
7.097e-03
    2      20    2.276809e+07    0.000e+00    1.804e+06
1.584e-02
    3      24    2.275305e+07    0.000e+00    5.564e+05
2.305e-02
    4      27    2.271959e+07    0.000e+00    1.200e+05
2.311e-02
    5      30    2.266221e+07    0.000e+00    3.345e+04
7.650e-04
    6      33    2.266187e+07    0.000e+00    1.614e+04
2.352e-04
    7      36    2.266187e+07    0.000e+00    1.764e+02
2.020e-04
    8      39    2.266186e+07    0.000e+00    3.768e+00
9.822e-07
    9      42    2.266186e+07    0.000e+00    9.319e-01
8.091e-09
   10      45    2.266186e+07    0.000e+00    3.962e+00
7.210e-08
   11      48    2.266186e+07    0.000e+00    6.485e-01
6.100e-08
   12      51    2.266186e+07    0.000e+00    7.598e-01
4.086e-09
   13      61    2.266186e+07    0.000e+00    7.588e-01
7.387e-09
   14      64    2.266186e+07    9.313e-10    1.037e+00
5.313e-09
   15      67    2.266186e+07    0.000e+00    1.147e+00
1.939e-09
   16      70    2.266186e+07    0.000e+00    1.598e+00
7.101e-09
   17      73    2.266186e+07    9.313e-10    2.220e+00
4.011e-09
```

```
   18      84    2.266186e+07    0.000e+00    6.613e-01
2.228e-09
   19     118    2.266186e+07    0.000e+00    6.613e-01
3.825e-17

Local minimum possible. Constraints satisfied.

fmincon stopped because the size of the current step is
less than
the selected value of the step size tolerance and con-
straints are
satisfied to within the selected value of the constraint
tolerance.

<stopping criteria details>

Resistance
1692.66

Total power at optimum
22661.86

Thrust difference to required at optimum
-0.00

Power division at initial guess :
102.94
98.53

Total power at initial guess :
22661.86

Thrust difference at initial guess :
6.86

Revs 1st CL 2nd POD, RPM
72.393
87.602

division power
MID SIDE
142.62
78.69

POwer total
22661.86

Vref MID, POD
1.908738
1.732295

J Values Mid, Pod
```

```
0.873509
0.969292
```

Appendix 2. Discretization Schemes

```
divSchemes
{
div(rhoPhi,U)   Gauss vanAlbada;
div(phi,alpha)  Gauss vanLeer;
div(phirb,alpha) Gauss linear;
div(phi,k)      Gauss vanLeer;
div(phi,omega)  Gauss vanLeer;
div(((rho*nuEff)*dev2(T(grad(U))))) Gauss linear;
}
```

Appendix 3. Boosting Results (Model Tests)

MODEL PROPULSION FACTORS
GROUP MID

SHIP MODEL NO. Model C 110%MID

VS KNOTS	VM M/S	NM HZ	FN	KQ	J
18.00	1.831	5.825	.156	.02592	0.919
22.01	2.239	7.091	.191	.02571	0.919

MODEL PROPULSION FACTORS
GROUP POD

SHIP MODEL NO. Model C 110%MID

VS KNOTS	VM M/S	NM HZ	FN	KQ	J
18.00	1.831	7.728	.156	.04038	0.925
22.01	2.239	9.409	.191	.04006	0.927

MODEL PROPULSION FACTORS
GROUP MID

SHIP MODEL NO. Model C 130%MID

VS KNOTS	VM M/S	NM HZ	FN	KQ	J
18.00	1.831	6.006	.156	.02786	0.893
22.01	2.239	7.311	.191	.02768	0.893

MODEL PROPULSION FACTORS
GROUP POD

SHIP MODEL NO. MODEL C 130%MID

VS KNOTS	VM M/S	NM HZ	FN	KQ	J
18.00	1.831	7.549	.156	.03865	0.949
22.01	2.239	9.190	.191	.03840	0.951

MODEL PROPULSION FACTORS
GROUP MID

SHIP MODEL NO. Model C 160%MID

VS KNOTS	VM M/S	NM HZ	FN	KQ	J
18.00	1.831	6.259	.156	.03039	0.858
22.01	2.239	7.621	.191	.03026	0.858

MODEL PROPULSION FACTORS
GROUP POD

SHIP MODEL NO. Model C 160%MID

VS KNOTS	VM M/S	NM HZ	FN	KT	KQ	KQ-O	J
18.00	1.831	7.273	.156	.1506	.03571	.03599	0.989
22.01	2.239	8.851	.191	.1505	.03561	.03597	0.990

MODEL PROPULSION FACTORS
GROUP MID

SHIP MODEL NO. Model C 200%MID

VS KNOTS	VM M/S	NM HZ	FN	KQ	J
18.00	1.831	6.576	.156	.03334	0.816
22.01	2.239	8.014	.191	.03325	0.815

MODEL PROPULSION FACTORS
GROUP POD

SHIP MODEL NO. Model C 200%MID

VS KNOTS	VM M/S	NM HZ	FN	KQ	J
18.00	1.831	6.869	.156	.03082	1.052
22.01	2.239	8.359	.191	.03091	1.051

NOTES:-FOR EXPLANATION OF ABBREVIATIONS SEE LIST OF SYMBOLS
-THE FACTORS ABOVE ARE MODEL VALUES AT THE SELF PROPULSION POINT OF SHIP CORRESPONDING TO A FRICTION CORRECTION DETERMINED BY THE ITTC-1957 FORMULA, 0.00028
A MODEL-SHIP CORRELATION ALLOWANCE OF C 12.8
AND A TEMPERATURE OF THE TANK WATER OF DEGREES C.
-THE PROPULSION FACTORS ARE BASED ON THRUST IDENTITY